Synthesis and Evaluation of 5-Fluorotriazole Cyclam Complexes as Target Activated Metal Complexes

Simon Barend Marais

School of Chemistry

Faculty of Science

The University of Sydney

A thesis submitted in fulfilment of the requirements for the degree

Master of Philosophy

December 2025

STATEMENT OF CONTRIBUTION

All melting points, infrared spectra, ultraviolet-visual spectra and the majority of ^{1}H and ^{13}C nuclear magnetic resonance spectra and low-resolution mass spectra were obtained by the author. Some low-resolution mass spectra and all high-resolution mass spectra were obtained by Dr. Nicholas Proschogo and associates of the Mass Spectrometry Facility, University of Sydney. Some ^{1}H and ^{13}C NMR spectra were obtained by Dr. Ian Luck and associates of the NMR Facility, University of Sydney. Proof reading and editorial advice was provided by Professor Peter Rutledge.

I, the author, interpreted all data. I produced all figures, tables, graphs, and schemes except where another source has been referenced. All synthetic chemical and biological procedures were carried out by the author.

I certify that this report contains work carried out by myself except where otherwise acknowledged.

Simon Barend Marais

STATEMENT OF ORIGINALITY

This is to certify that the content of this thesis is my own work. This thesis has not been submitted for any other degree or purpose.

I certify that the intellectual content of this thesis is the product of my own work, and that all assistance received in preparing this thesis and all sources have been acknowledged.

Simon Barend Marais

No content produced by generative AI tools has been used in the preparation of this thesis.

This research was supported by an Australian Government Research Training Program (RTP) Scholarship.

Acknowledgements

Firstly, I would like to thank my supervisor Professor Peter J. Rutledge, for giving me the opportunity to work on this project with him over the last four years. He has provided me excellent guidance and constant motivation when things weren't going my way synthetically. I also appreciate him letting me go part time to focus on myself as well as proof-reading my thesis many times. I will definitely miss talking about the cricket and rugby during our catch ups and how South Africa is always better than New Zealand 😊, followed by a run-down on the chemistry throughout the fortnight.

To all the members of the Rutledge group past and present, Julius thank you for all your time when I first started in the lab, I understand that someone constantly nagging you for help can be frustrating, but your patience was much appreciated. Klem, I will miss our weekly updates on the weekend, life in general and a sprinkle of chemistry. Will, thank you for taking time out of your weekends to read the first draft of my thesis chapters!! B and Eddy, I will never forget all the fun we had, I think we all kept each other sane, and the constant jokes and funny discussions made me excited to come to the lab. Thanks for looking after me when I was the only one from the Rutledge group present. To Nick, Bella, Liz, Susanna, Lorenzo, Kymberley, thanks for making the lab such a great place to work.

To the technical staff of the School of Chemistry, thank you so much for keeping everything running smoothly. Nick, thank you for all your assistance with MS and all the advice you have given me. Ian and Paige, thank you for keeping the NMR machines up and running and to Tahmineh for keeping the lab running smoothly and the service room stock constantly full.

Finally, to my mum, Martin, Wilhelm, Anna, baby Benji, my girlfriend Mon and all my friends, thank you for your continuous love, support and for letting me be myself. I definitely could not have done this without you.

To my dad, your own fight was the inspiration for this work, I hope you are proud.

Contents

Abbreviations

Boc	tert-Butyloxycarbonyl
CCD	Cyclam-functionalised carbon dots
CO-ADD	Community for Open Antimicrobial Drug Discovery
CT	Computed topography
CuAAC	Copper(I)-catalysed azide alkyne cycloaddition
CV	Column volume
DCM	Dichloromethane
DMS	Dimethylsulphate
DMSO	Dimethyl sulfoxide
ENDOR	Electron-nuclear double resonance
EPR	Electron Paramagnetic Resonance
ESI	Electrospray ionisation
EtOAc	Ethyl acetate
EtOH	Ethanol
GCA	Gadolinuim-based contrast agent
HEPES	4-(2-Hydroxyethyl)piperazine-1-ethanesulfonic acid
HER	Human estrogen receptor
HF	Hydrogen fluoride
KF	Potassium fluoride
NMR	Nuclear magnetic resonance
LC	Liquid chromatography
LRMS	Low resonance mass spectroscopy

MALDI	Matrix-assisted laser desorption/ionisation
MeOH	Methanol
MeCN	Acetonitrile
MMP	Matrix metalloproteinase
MRI	Magnetic resonance imaging
MS	Mass spectrum/spectra
m.p.	Melting point
NSF	Nephrogenic systemic fibrosis
PET	Photoinduced electron transfer
PPi	Diphosphate
PR	Progesterone receptor
POC	Proof of concept
rt	Room temperature
SWI	Susceptibility-weighted imagine
TAMC	Target-activated metal complexes
TEA	Triethylamine
THF	Tetrahydrofuran
TMEDA	Tetramethylethylenediamine
Tosyl	4-Toluenesulfonyl

Abstract

Metal containing drugs remain an important class of compounds due to their exquisite potency, however their clinical use is often limited by poor selectivity. The overall aim of this thesis is to develop and investigate cyclam fluorotriazolyl derivates for sensing applications by exploiting the versatile metal-binding capability of cyclam and the synthetic simplicity of the CuAAC reaction to obtain target triazolyl derivatives. A variety of metal-cyclam-based systems have been investigated for potential in monitoring triazole connectivity and biological binding events.

In Chapter two, an efficient synthesis of 5-fluorotriazole-cyclam metal complexes has been developed in which the pendant group is connected to cyclam via N1. A halogen-exchange protocol has been used to access fluorinated-triazole systems. ^{19}F NMR and ^{1}H NMR confirm the presence of conformational isomers.

In Chapter three, ligand-induced displacement of the pendant triazole from the metal centre of the complexes described in Chapter two was used to simulate changes to the metal coordination environment as were observed upon binding of biotinylated cyclam complexes to avidin. Mass spectrometry and ^{19}F NMR spectroscopy confirm successful triazole displacement.

Collectively these results establish 5-fluorotriazole-cyclam complexes as promising molecules for ^{19}F-based coordination sensing. This work provides a foundation for applying ^{19}F NMR as a sensitive and versatile method for probing more complex coordination events in biological systems.

Chapter 1 – Introduction

1.1 Metals in Medicine

Metals have played a role in medicine for centuries, but the modern era of metallodrugs began in 1909 with the discovery of salvarsan, an arsenic-based compound used to treat syphilis.[1] Since then, metal-based drugs have played a crucial role in modern medicine with a growing scope of applications. Metal-based therapeutics harness the chemical properties of metal ions - redox activity, variable coordination, and catalytic reactivity - to target diseases in ways that organic drugs often cannot.[2] However, this chemical versatility comes with a cost: poor selectivity. The same features that make metal complexes reactive readily cause off-target toxicity. [3] The common, unintended side-effects of metallodrugs are a consequence of their versatile activation pathways and multi-targeting capabilities, as the compounds often interact with a diverse range of biomoleclues.[4] While the most iconic example of a metallodrug remains *cis*-platin - a platinum-based complex used extensively in chemotherapy- the therapeutic scope of metallodrugs has expanded significantly over the last few decades.[5] Metallodrugs now encompass compounds with antiviral, antibacterial, diagnostic and antineoplastic applications.

A key area of interest is the development of metal complexes as antibiotics. Highlighted by Frei *et al*. in a review which analysed 906 metal-containing compounds incorporating 29 different metal elements for their antifungal and antibacterial activity.[6] Of the 906 metal-containing compounds screened by the Community for Open Antimicrobial Drug Discovery (CO-ADD), 88 compounds showed activity against at least one of the tested strains, a hit-rate of 9.9%. Purely organic molecules in the CO-ADD database only exhibited a hit-rate of 0.87%, a significantly lower hit-rate than metal-bearing compounds. Nearly 75% of the 'new' antimicrobials currently in clinical development are simple derivatives of existing antibiotics, so they are likely to remain vulnerable to established resistance mechanisms. Moreover, the number of pharmaceutical companies actively pursuing antibiotic research declines each year due to poor return on investment, so the commercial development of new antibiotics is unlikely to meet growing demand.[7] The review by Frei *et al*. underscores the significant potential of metal-based compounds to address antimicrobial resistance through novel mechanisms and chemical diversity beyond that of conventional organic molecules.

While these metal complexes show great promise, Frei *et al*. also highlights the significant number of metal complexes that are cytotoxic.[6] Only 30 of the complexes that showed activity

against strains were non-toxic and non-haemolytic to mammalian cells at the same concentration. Furthermore, the metal complexes screened that contain readily accessible elements like iron returned no possible antibiotic capabilities due to toxicity. While palladium, iridium, platinum and silver complexes showed promising activity, these elements are expensive, which potentially limits their use in clinical antibiotics if large doses are required.

Beyond antimicrobial applications, radiopharmaceuticals constitute another major class of metal-based drugs. Metal-containing compounds have long played a critical role in positron emission tomography (PET), which provides functional imaging data complementary to anatomical information obtained from magnetic resonance imaging (MRI) and computed tomography (CT).[8] In 1988, gadopentetate dimeglumine ($[Gd(DTPA)]^{2-}$) became the first gadolinium-based contrast agent (GCA) approved for clinical use.[9] This compound significantly improved MRI by enhancing soft tissue contrast via its strong paramagnetic effect, which accelerates T_1 relaxation of nearby protons. Since then, extensive research has been devoted to developing metal-based contrast agents. In addition to gadolinium, other metals such as iron, gold, and manganese have been explored; however, gadolinium remains the primary focus due to its strong paramagnetic properties. For example, Ceballos-Ceballos *et al*. reported that gadolinium-enhanced susceptibility-weighted imaging (SWI) MRI achieved approximately twice the lesion detection rate compared to non-contrast scans.[10] Additionally, Panagiotidis *et al*. investigated the clinical utility of gadolinium- and fluorine-based contrast agents in PET/CT imaging of 104 patients with neuroendocrine tumors.[11] The gadolinium-based tracers offered distinct diagnostic advantages, resulting in modified treatment strategies in 81% of cases. These examples underscore the essential role of metal-containing agents in advancing molecular imaging and enabling more precise clinical decision-making; however, their use is also not without risk.

GCAs have been strongly associated with nephrogenic systemic fibrosis (NSF), a rare but serious condition characterized by progressive fibrosis, muscle weakness, joint contractures, and, in severe cases, permanent disability.[12] These safety concerns have raised regulatory scrutiny and limit the widespread use of certain GCA formulations, particularly in patients with impaired renal function, where the risk of NSF is highest.[13]

In addition to their roles in antimicrobial and diagnostic applications, metal complexes have also proven invaluable as antineoplastics for the treatment of cancers. First licensed for medical use in 1978, the platinum-based anti-cancer drug *cis*-platin is still used as a first-line therapy

and is highly effective in the treatment of ovarian, bladder, head and neck cancers.[5] The efficacy of *cis*-platin is linked to its hydrolysis: once the drug enters the cell, the ligand undergoes aquation whereby a water molecule displaces a chlorine.[14] Subsequent binding of the drug occurs when the *N*-heterocyclic base guanine displaces the water molecule, leading to crosslinking *via* further displacement of the other chlorine atom.[3] (Figure 1)

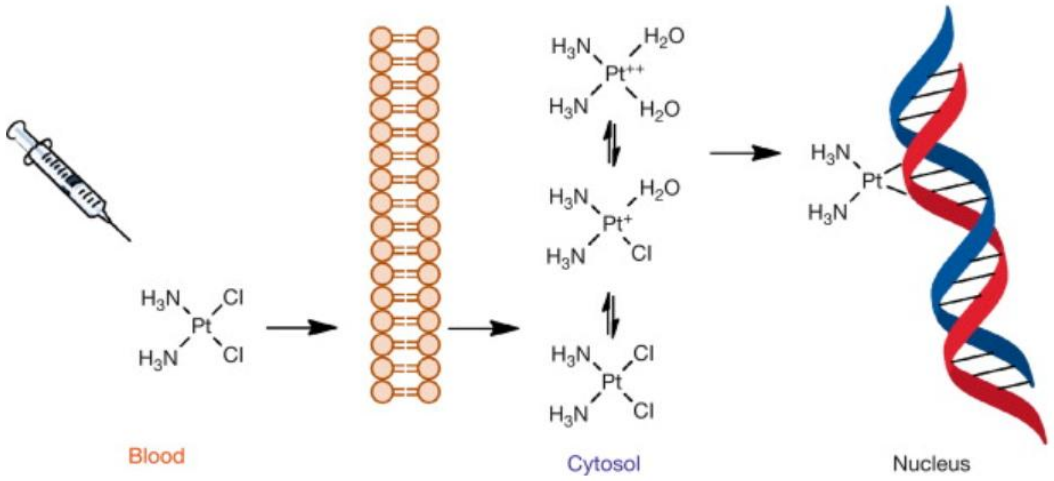

Figure 1: The binding of *cis*-platin to the N-heterocyclic base guanine, leads to crosslinking, limiting DNA processing.[15]

Crosslinking of nuclear bases disrupts DNA repair mechanisms, leading to DNA damage and ultimately inducing apoptosis in cancer cells.[16] While potent, *cis* -platin lacks selectivity and also interacts with a variety of intracellular biomolecules.[17] This lack of selectiveness, means that *cis*-platin brings significant side effects, including hearing and neurological deficits for patients.[18] Furthermore, *cis*-platin is excreted via the urine, which drastically increases the concentration of platinum in the kidney and leads to nephrotoxicity in over 30% of patients.[19]

While the therapeutic and diagnostic potential of metal-based compounds is increasingly evident, ranging from their role in combatting antimicrobial resistance to enhancing the sensitivity and specificity of medical imaging, their clinical use is not without limitations. Many metallodrugs, particularly those involving heavy or lanthanide metals, pose risks related to toxicity, off-target effects, and bioaccumulation. The significant side effects associated with many metal-based drugs means that utilization in treatments is often approached with caution. To overcome selectivity challenges, we can look to biological systems for inspiration and use synthetic tools to engineer safer metallodrugs.

1.1.1 Modulating Metal Reactivity Using Ligands

Previous work in the Rutledge and Todd groups has investigated biologically inspired systems designed to control metal reactivity and create more selective metallodrugs with fewer side effects.[20, 21] These biologically inspired systems utilise click chemistry to create triazole linkers between macrocycles and target ligands. The term 'click' chemistry was first used by Barry Sharpless to describe simple efficient reactions that are highly powerful and selective. One of the most versatile 'click' reactions is the copper(I)-catalysed azide-alkyne cycloaddition (CuAAC) which allows for the quick, high yielding synthesis of 1,4-disubstituted 1,2,3-triazole derivatives.[22] The CuAAC reaction of terminal alkynes selectively generates 1,4-disubstituted triazoles (Figure 2).[23]

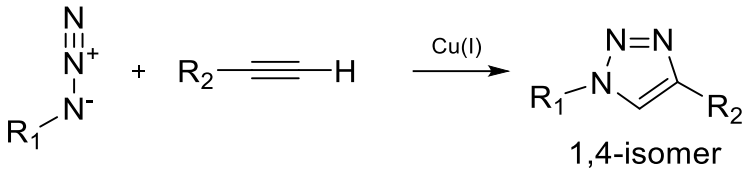

Figure 2: CuAAC reaction between an azide and alkyne forming solely the 1,4- disubstituted regioisomer.[23]

'Click' chemistry has been used by the Rutledge Group to incorporate a variety of bio-ligands and drugs onto a macrocyclic core. Previous work in the group has included making derivatives of Marimastat, a matrix metalloproteinase (MMP) inhibitor that failed clinical trials due to the negative side effects arising from its poor target selectivity.[20] Derivatives in which Marimastat is appended to a macrocyclic core resulted in only a slight inhibition of activity relative to the parent compound, demonstrating the potential of metal-macrocycle complexes for the investigation and treatment of diseases.

Beyond therapeutic and diagnostic applications, metal-ligand complexes also play a critical role in chemical sensing. Their unique coordination chemistry and spectroscopic signatures make them ideal candidates for the selective detection of biologically and environmentally relevant analytes.[24] In particular, macrocyclic scaffolds-previously explored for drug delivery-can be repurposed as highly tuneable sensing platforms. The following section explores the development of such metal-based systems for chemical sensing applications, with a focus on their design, mechanism of detection, and analytical performance.

1.2 Chemical Sensing

Chemical sensors provide analytical data about a system. They typically consist of two components, a receptor and a transducer (Figure 3).[25] A chemosensor is a molecule that interacts with an analyte through a receptor to initiate a signal in the transducer.[26] The analyte is typically the species of interest, and analysis of the transducer signal can yield useful information about a biological target.[27, 28] As chemosensors are molecular, synthetic modifications can be made to alter the selectivity of the receptor and the sensitivity and output of the transducer. Diverse chemosensors have been developed for a wide range of applications, featuring highly varied structures. The malleable nature of chemosensors allows for the creation of hyper-specific and sensitive sensors with targets ranging from anions and cations to hazardous materials and biologically important molecules. [29-31]

Upon binding of the analyte to the receptor, the initiation and output of the transducer is most commonly an optical or electrochemical signal.[32] Optical sensors can be monitored based on receptor type: a UV-visible instrument for colorimetric sensors and fluorescence spectroscopy for fluorometric chemosensors.[29] Electrochemical change due to a change in redox potential can be monitored by voltammetry.

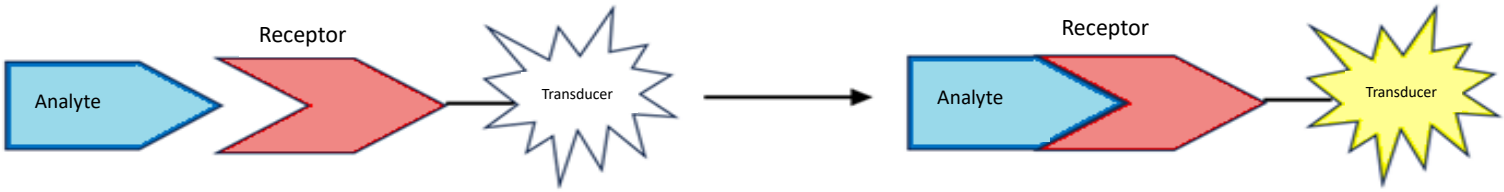

Figure 3: A schematic representation illustrating the interaction between analyte and receptor, resulting in a detectable signal in a transducer.

Chemical sensors find diverse applications across industries including medical, environmental, and industrial sectors. For example, DNA based biosensors rapidly detect a small number of microbes with high sensitivity and selectivity.[33] Dual chemosensors for zinc and cadmium ions provide highly specific low-cost fluorescent sensors which are used for real-time detection of pesticides and herbicides,[34] minimizing their adverse impact on the environment.[35] Industrial practices utilise chemical sensors to determine the completion of processes, for example, monitoring levels of dimethylsulphate (DMS), a carcinogenic substance used as a methylating agent in the production of dyestuffs. Sensors are employed to investigate the closed system,

indicating reaction completion and ensuring hydrolysis of all excess DMS, resulting in increased yields and a safer work environment.[36]

1.2.1 Cyclam-based Sensors

Cyclam is a 14-membered tetraamine macrocycle that can complex transition metals, with high kinetic and thermodynamic stability.[37] The strong cation binding has been attributed to a combination of both enthalpic and entropic effects.[38] Cyclams have found a variety of uses in chemical sensing and other applications.[39-41]

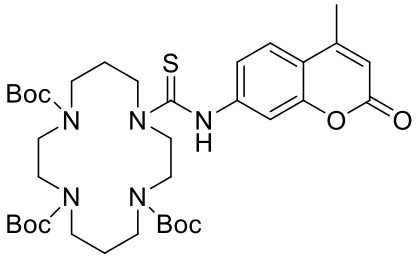

1

Figure 4: Structure of Hg^{2+} sensor **1**.

The substituted cyclam complex **1** has been utilised as a 'turn on' fluorescent sensor which coordinates selectively to mercury ions in solution (Figure 4). The ensuing change in fluorescence profile enables accurate measurements of ion concentrations:[42] both excitation and emission spectra increase in signal intensity relative to mercury concentration. Competition studies with various ions found that Hg^{2+} binds with the same affinity regardless of the presence of competitive ions. This high selectivity was proposed to be due to the weaker interaction of Hg^{2+} with electron pairs on the amide/thioamide macrocyclic nitrogens which is supplemented by additional interactions between the sulphur atom and the oxygen species in the Boc groups.

Many other cyclam complexes have been deployed to detect ions that could potentially induce harmful effects on the body. For example, the detection of Cu^{2+} and S^{2-} ions has been tested on a highly sensitive fluorescent sensor comprising of cyclam-functionalised carbon dots (CCDs).[43] The CCDs displayed excellent selectivity and sensitivity toward Cu^{2+} ions, even in solutions containing competing ions. The highly selective sensor effectively determined the concentration of Cu^{2+} ions in both blood serum and tap water. Additionally, its low cytotoxicity enabled successful imaging of Cu^{2+} and S^{2-} ions in live HeLa cells.

Previous work in the Rutledge and Todd groups has reported several cyclam based chemosensors for metal ions, utilising the CuAAC reaction to create a triazole linker between the fluorophore and cyclam component of the molecule.[44, 45] (Figure 6)

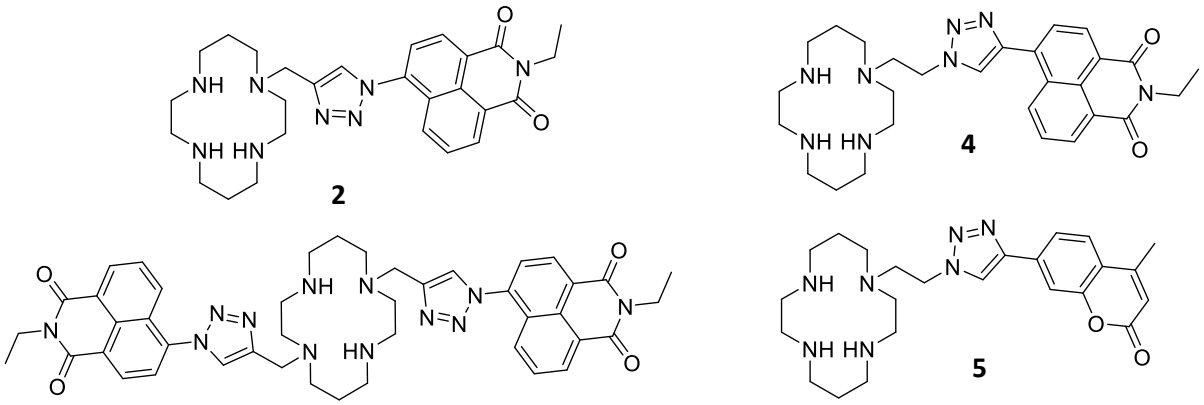

Figure 5: Structure of Zn^{2+} sensors **2**, **3** and **5**, and Cu^{2+}/Hg^{2+} sensor **4**.

Tamanini *et al*. explored the potential of mono- and bis-naphthalimide cyclam complexes **2** and **3** as sensitive Zn^{2+} sensors.[44] The mono substituted complex **2** exhibited excellent selectivity for Zn^{2+} in aqueous solutions of varying pH (> 4.5), showing a 6-fold enhancement in emission upon zinc binding. The Cu^{2+} and Hg^{2+} cations demonstrated similar quenching. The efficacy of this complex was shown in the detection of Zn^{2+} concentrations in apoptotic thymocytes. Moreover, the addition of the second naphthylamide unit **3** resulted in a doubling of fluorescence intensity compared to the mono substituted in response to Zn^{2+}, with a more than 12-fold increase in measured emission.

Lau *et al*. reported an 'on-off' response by cyclam sensor **4** which contains '*reversed'* triazole connectivity from cyclam to a coumarin fluorophore.[45] The '*reversed'* triazole connectivity involves the pendant fluorophore attached to the C4 of the triazole (and the macrocycle to C1). Complex **4** was employed to differentiate between Hg^{2+} and Cu^{2+} ions in solution and displayed excellent selectivity towards Cu^{2+} and Hg^{2+} in competition experiments with other cations. The observed quenching of fluorescence was attributed due to heavy metal and paramagnetic effects. Differentiation between Cu^{2+} and Hg^{2+} was achieved through the addition of anions to effect 'fluorescence rescue' with the Hg^{2+} complex only. ^{1}H NMR and MS experiments revealed that the anion triggers demetallation of the Hg^{2+} complex, leading to the revival of fluorescence.

Ast *et al*. further explored the effect of the triazole connectivity on the fluorescence properties of sensors.[46, 47] A mono-naphthalimide probe **5,** featuring C4 triazole connectivity, was utilised and exhibited a similar response to the presence of zinc, showing comparable 5-fold enhancement of fluorescence emission when compared to compound **2**. However, the change in triazole connectivity brought a 10-fold increase in quantum yield and a 6-fold increase in lifetime measurements when compared to **2.** To determine the mechanistic basis for fluorescence enhancement, Cu^{2+} and Zn^{2+} complexes of both coumarin **4** and naphthalimide **5** derivatives were tested at lower temperatures. It was found that photoinduced electron transfer (PET) was responsible for the fluorescence response to Zn^{2+} and energy transfer was responsible for quenching by Cu^{2+}.

1.2.2 Developing Target Activated Complexes to Respond to Biomolecules

Taking the potential of cyclam complexes as chemosensors a step further, Tamanini *et al*. proposed the idea of sensing biological macromolecules by manipulating and monitoring the coordination geometry of metal centres within so-called 'Target-Activated Metal Complexes' (TAMCs).[44] TAMCs are metal complexes that remain unreactive and unresponsive until they reach their intended target. At this point biomolecule binding renders a structural change in the coordination of the complex, initiating a signal output or change in reactivity.

In a first approach Tamanini *et* al. recorded changes in the electron paramagnetic resonance (EPR) spectrum of a biotinylated TAMC, to monitor the interaction between biotin and avidin.[48] The copper complex **6** was prepared in which a cyclam macrocycle is connected to biotin via a triazole linker. Avidin was introduced and EPR used to monitor the changes in metal coordination. A difference in the EPR spectrum indicated a change in Cu^{2+} coordination from five-coordinate to a four-coordinate square planar. Using electron-nuclear double resonance (ENDOR) spectroscopy, Tamanini confirmed that it was the axial triazole nitrogen donor to copper that was lost. Further work by Lau *et al*. suggested that this change in coordination geometry occurs due to a steric interaction between the ligand and the bulky analyte forcing the dissociation of the triazole ligand from the metal centre.[21]

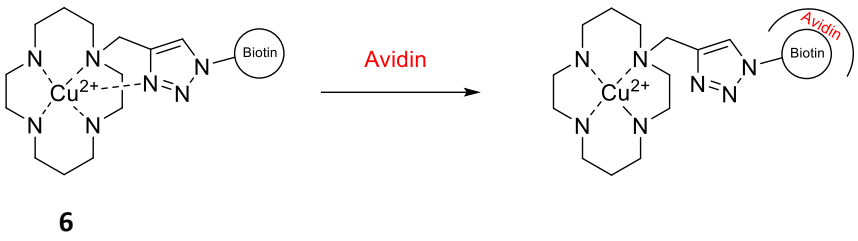

6

Figure 6: Initial concept of "scorpionand" ligand **6** binding to avidin.

The poor signal to noise ratio of the EPR spectroscopic measurements, compromised the efficacy of this approach for studying the biotin-avidin complex experimentally. So Yu *et al*. incorporated the high sensitivity and selectivity of fluorescence as an alternative to explore the interaction between biotin and avidin in a further proof-of-concept experiment.[49]

Complex **7** contains a triazolyl-naphthalimide ligand and a biotin ligand, plus a Zn^{2+} ion, as previously explored for fluorescence spectroscopy. This enabled further investigation and visualisation of the binding event between biotin and avidin using fluorescence spectroscopy. Fluorescence titrations were used to explore the binding of the complex **7** to avidin. Titration of complex **7** into a solution of avidin in 4-(2-Hydroxyethyl)piperazine-1-ethanesulfonic acid (HEPES) buffer resulted in a decrease in fluorescence intensity compared to control experiments, attributable to the binding of avidin to complex **7.**

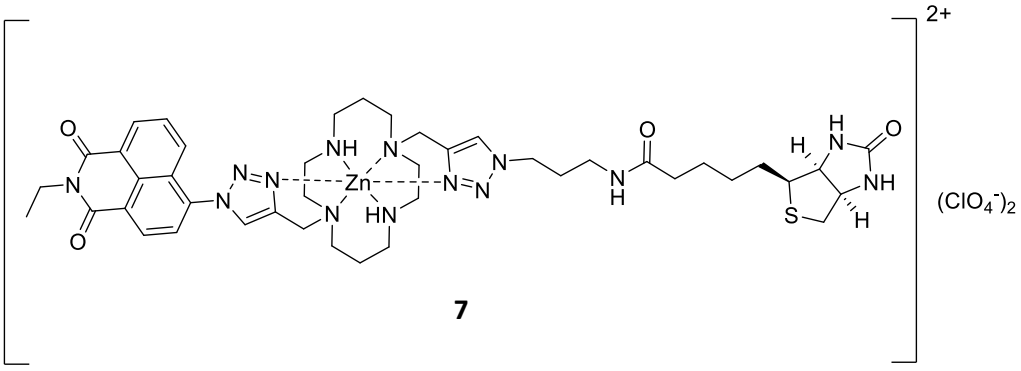

7

Figure 7: Structure of the biotinylated cyclam complex **7**.

A plot of emission intensity vs [**7**: avidin], shows this effect clearly, up to the addition of 4 equivalents (as consistent with known biotin:avidin binding stoichiometry) confirming that this fluorescence change occurs due to the binding of avidin to biotin. (Figure 8)

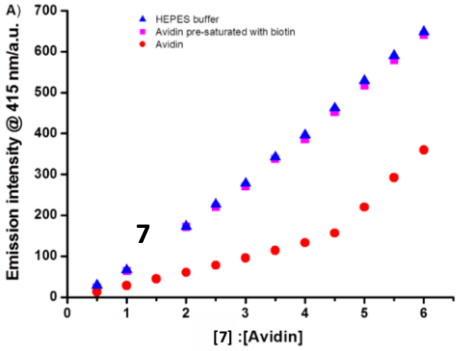

Figure 8: Fluorescence response of **7** in response to both avidin and controls.

Yu *et al*. proposed two possible explanations for the decrease in emission of the avidin-bound metal complex relative to the complex itself in solution. Firstly, amino acid residues in the biotin binding pocket could quench the fluorescence of the dye. Previous work confirmed that the fluorescence of unmetalated biotin-dye conjugates is quenched upon avidin binding.[50] The other explanation invokes a coordination change at the Zn^{2+} ion, resulting in a knock-on effect on the fluorophore.[49] Since the binding of the avidin alters the coordination of the metal (as demonstrated by EPR and ENDOR), this change may also affect fluorescence output. The mono-naphthalimide complex exhibits half the fluorescence intensity of the bis- naphthalimide complex, hence binding of avidin to biotin may cause an agitation of the coordination environment.

1.2.3 Targeting the '5th' position of the Triazole

As a next step Wong *et al*. investigated the idea that NMR spectroscopy might provide a more versatile and simpler method for probing metal coordination geometry, aiming to overcome the poor signal-to-noise ratio of the EPR/ENDOR methods previously reported,[51] and resolve the uncertainty over the reasons behind the fluorescence changes observed within complex **7**. NMR spectroscopy could also enable the validation of the target-activated "allosteric scorpion" mechanism proposed by Tamanini. Wong *et al*. confirmed that the addition of chloride or

related species could selectively displace the triazole from the metal in select complexes (first reported by Lau *et* al. in 2011)[45] and that this could be monitored by ^{1}H NMR spectroscopy.

Additionally, using ^{2}H NMR on specifically deuterated complexes (**9**) (Figure 9) enabled the coordination change to be monitored in a noisy ^{1}H landscape. This approach addresses the anticipated challenge that protein-derived ^{1}H signals will overlap with the key triazole signal in experiments with biomolecular binders, thereby ensuring effective monitoring of changes in metal coordination in more complex systems, such as the biotin-avidin system. Given the low abundance of deuterium in nature,[52] the inclusion of deuterium in the molecule provides a highly selective method of monitoring changes within the complex.[51]

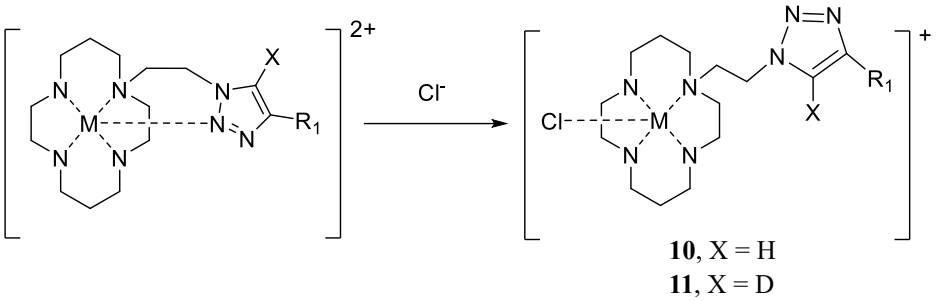

Figure 9: Anion induced displacement of triazole complex **8** and **9**.

To make deuterated compounds, click reactions were performed in the presence of D_2O as a co-solvent alongside THF to obtain both N1 and C4 triazole connectivity complexes deuterated at the unsubstituted triazole C. Conducting ^{2}H NMR experiments with the C4 complex **9** in the presence and absence of chloride anions, revealed a discernible upfield shift of the triazole peak from δ = 8.69 to 8.49 ppm which provided good agreement with the results obtained in the ^{1}H NMR investigation. This provided evidence that the ^{2}H NMR could provide useful results in the investigation of more complex binding experiments *in vivo.*

Whilst the ^{2}H NMR provided a greater ease of detection for metal coordination changes, the inherently low sensitivity of ^{2}H NMR in comparison to ^{1}H NMR is potentially problematic in other studies where a lower concentration of complex is required.

1.2.4 5-Fluorotriazoles

To circumvent the low sensitivity of ^{2}H NMR spectroscopy, we envisage that this concept could be further extended to take advantage of the greater sensitivity and contrast afforded by ^{19}F NMR by using F-labelled triazoles. The sensitivity of a fluorine nucleus to the local environment is much greater for fluorine than for hydrogen (or deuterium).[53] Furthermore,

fluorine is entirely absent from most biomolecules, greatly enhancing signal:noise considerations in protein binding experiments, and meaning that a change in fluorine environment could be easily monitored. A selectively mono-fluorinated probe would only contain the singular fluorine atom, meaning that ^{19}F NMR would allow the one signal arising to be monitored exclusively for changes in the local fluorine environment, providing a much more reliant monitoring method.

Fokin *et al*. first achieved the efficient synthesis of 5-fluoro-1,2,3-triazoles through halogen exchange reactions with 5-iodotriazoles,[54] building on the work of Hein *et al*. who first investigated the potential of 1-iodoalkynes as 'click' partners in reactions with organic azides to selectively produce 5-iodotriazoles in excellent yields.[55]

Iodoalkynes can be synthesized using a simple and highly efficient method that involves treatment of terminal alkynes with *N*-iodomorpholine in the presence of Cu(I). Iodoalkynes exhibit exceptional reactivity with organic azides in the presence of a Cu(I) catalyst, surpassing even the reactivity of terminal alkynes.[55] Inclusion of the amine ligand triethylamine (TEA) is crucial and ensures generation of solely the 5-iodotriazole product in high yield (90%) when 2 equivalents of the base are used.

Fokin *et al*. demonstrated that potassium fluoride (KF) and acidic potassium bifluoride (KF_2) are effective fluoride sources for converting 5-iodotriazoles to their fluoro counterparts.[54] KF showed good compatibility with 5-iodotriazoles that also contain heterocycles, chlorides, acetals and alcohols functionality, whilst KF_2 demonstrated good compatibility with amides, nitriles and ketones. Both fluoride sources are effective under the same reaction conditions, which involved a 1:1 solvent mix of MeCN/H_2O and heating in a microwave reactor at 180°C for 10 minutes. (Figure 15) It was also noted that an aromatic group is required in the 4-position of the triazole for effective transformation from 5-iodotriazole to 5-fluorotriazole: due to the complex variety of products that arose when aliphatic substituents were present at this position. Additionally, when 1,3-triazoles or 1,2-triazoles were exposed to the same conditions, no conversion of the iodotriazole to the fluorotriazole was observed. This is thought to be due to the ability of 1-4 iodotriazoles to undergo ring-chain isomerization or an aromatic nucleophilic substitution reaction.

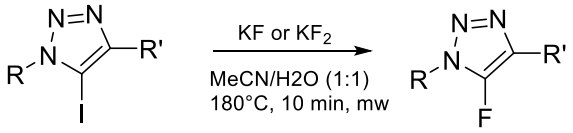

Figure 10: General synthesis of 5-fluoro-1,2,3-triazoles from 5-iodo-1,2,3-triazoles utilising KF and KF_2.[54]

Since the reaction conditions by Fokin *et al*. were harsh and required an aromatic group in the 4-position of the triazole as well as an aliphatic substituent on N1 for efficient halogen exchange, Chu *et al*. investigated milder reaction conditions that would allow a broader substrate scope for the efficient synthesis of 5-fluorotriazoles.[56] Their optimised conditions involve heating a triazole substrate with 5 equivalents of AgF and 0.5 equivalents of tetramethylethylenediamine (TMEDA) in toluene at 120°C. These conditions were successfully deployed with a wide range of 5-iodotriazoles bearing both electron-rich and electron-poor substituents. This method requires the exclusion of water for high yields as the reaction is thought to proceed via a bimetallic Ag^{2+} intermediate.

Crousse *et al*. have investigated routes to 5-fluorotriazole amino acid derivatives,[57] (Figure 11) by building on the Chu conditions. Using those conditions directly led to only detection of side products, as excess fluoride destroyed the substrate. However, by lowering reagent stoichiometries, Crousse *et al*. ascertained that 1.2 equivalents of AgF and 0.2 equivalents of TMEDA in toluene at 120°C afforded the desired products, albeit in lower yields. Further experiments to determine the effect of fluorine on the triazole, indicated that the presence of fluorine on the triazole does not significantly alter the behaviour of the triazole nucleus.

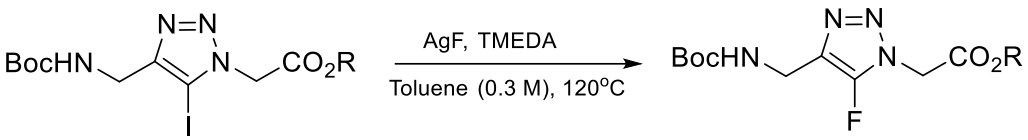

12 **13**

Figure 11: General synthesis of 5-fluoro-1,2,3-triazoles **13** from 5-iodo-1,2,3-triazoles **12** utilising AgF and TMEDA.[57]

1.2.5 ^{19}F-labelled sensors

Gan *et al*. reported the first ^{19}F-NMR labelled molecular sensor capable of detecting the presence of biologically significant phosphate anions using fluorine NMR.[58] The compound **14** (Figure 12) is a Zn^{2+}-dipicolylamine coordination complex with a fluorine atom attached to the para carbon of the bridging diamine. Compound **14** was mixed with equal amounts of two competing anions to determine its relative affinity for these analytes. Changes in the ^{19}F NMR spectra upon binding of the anions showed that diphosphate (PPi) causes the largest change in

the fluorine environment (21.5 ppm to 17.8 ppm). ATP (22.0ppm), ADP (20.5ppm), or phosphate (21.3 ppm) trigger much more modest spectroscopic changes. This demonstrates the sensitivity of ^{19}F NMR as a visualisation tool, as a binding event five atoms distant can be easily monitored.[59]

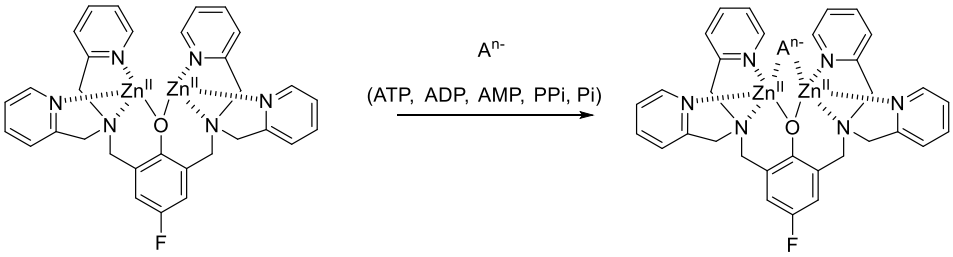

Figure 12: Structure of Zn^{2+}-dipicolylamine complex **14**.[58]

Applying this system, Smith *et al*. tracked the hydrolysis of ATP over time, demonstrating that conversion of ATP to ADP occurs within just 12 minutes, while the subsequent hydrolysis of ADP is significantly slower, taking over 41 hours. This work highlights the potential of ^{19}F labelled molecular probes for monitoring biological reactions.

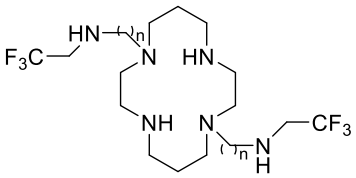

Figure 13. Structure of trifluoroethyl cyclam ligand **15**.[60]

In one further example Hermann *et al*. explored the potential of cyclam-based Cu^{2+} complexes to act as a ^{19}F MRI contrast agent.[60] The ligand **15** comprises a cyclam macrocycle with pendant trifluoroethyl amine ligands of varying length. Upon complexation with Cu^{2+}, the signal of the major and minor isomers could be accurately followed using ^{19}F NMR, allowing Hermann *et al*. to monitor protonation of the side arm amino groups in the complex relative to the free ligand. Protonation/deprotonation of the pendant amino groups can be monitored by ^{19}F NMR signals as the pH of the solution is varied, by comparing ^{19}F signals between the free ligand and the Cu^{2+} complex. The protonated amine will not coordinate to the central Cu^{2+} ion while the non-protonated form can bind to the metal, with consequent changes in ^{19}F signals. In the

compound with a 1,2-ethylene spacer for example, the pendant amino groups are coordinated to the metal at pH above 5. This complex also exhibits short relaxation times, at clinically relevant temperatures suggesting good scope for practical utilisation in ^{19}F NMR-based MRI imaging.

1.3 The Human Estrogen Receptor

Breast cancer is the most commonly diagnosed cancer in Australia with 1 in 7 women diagnosed with this form of cancer in their lifetime.[61] With over half a million deaths from breast cancer worldwide in 2020, it is clear that this is a serious issue in healthcare.[62] In 1950, Elwood Jensen first identified the human estrogen receptor (hER) as a determining factor in the propagation of breast cancer.[63]

Estrogen receptors are primarily located in the tissue of the female reproductive tract and the breast, but are also present in several other tissues such as bone, brain, liver and skin.[64] Estrogen plays a vital signalling role in several biological processes, including the menstrual cycle, pregnancy and menopause.[65]

Breast tumours can be estrogen receptor positive (ER+), progesterone receptor positive (PR+) or both (ER/PR+), indicating that the cancer responds to signals from these hormones to grow.[66] Estrogen receptors are expressed in 6 – 10% of healthy breast cells, but are overexpressed in approximately 70% of breast cancers.[67]

Estradiol acts as the primary agonist for the estrogen receptor and is the main steroid that binds to the hER, triggering transcription of genes that stimulate the proliferation and survival of breast cancer tissues.[68]

Since the hER is so heavily involved in the propagation and proliferation of breast cancer, it has become a key target for diagnosis and treatment of breast cancer.

16 **17**

Figure 14: Structures of estradiol (E2) **16** and 17α-ethynylestradiol **17.**

Being able to accurately determine the presence and upregulation of the hER in breast cancer tumours is an important factor in diagnosis and allows more accurate prediction of a given tumour's response to hormonal therapy.[67] One of the most commonly used tools for diagnosis of breast cancers is a biopsy, an invasive technique that carries risks of infection, can be painful and can occasionally disrupt the tumour's microenvironment.[69] Other measures to safely and less invasively screen the body for breast cancer tumours are desired.

1.3.1 Imaging the Human Estrogen Receptor

Since the 1980s, many groups have evaluated steroidal and non-steroidal compounds for hER imaging in patients. Notably, Kieswetter *et al*. developed ^{18}F-fluoroestradiol ([^{18}F] FES) as a radiopharmaceutical alternative for molecular imaging in 1984.[70] [^{18}F] FES binds to the hER within the body and accumulates in hER-rich tissue. Positrons emitted as the fluorine-18 decays, interact with the electrons in the body, producing gamma rays that are detected by a PET scanner. Various studies have shown [^{18}F] FES has good selectivity and uptake in tumours and is a useful tool for monitoring hormonal therapy. In May 2020, the FDA approved the use of [^{18}F] FES in PET imaging for the detection of ER+ lesions and to assist biopsy techniques in patients with recurrent breast cancers.

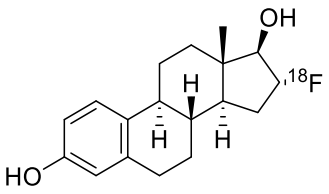

18

Figure 15: Structure of [^{18}F] FES **18**.

Tejería *et al*. used click chemistry with 17α-ethynylestradiol **17** to synthesize a [^{18}F]-labelled estradiol derivative for applications in estrogen receptor imaging.[67] Click chemistry enables the synthesis of precursors for radiolabelling by installing 'prosthetic' groups for radio halogenation. Tejería *et al*. developed the [^{18}F]-labelled molecule [^{18}F]F-FEET **19** which maintained the commonly accepted pharmacophore structure for a hER antagonist, including the rigid hydrophobic skeleton, the presence of the aromatic ring, and 2 OH groups with 11Å between their oxygen atoms.

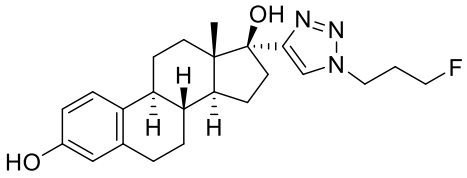

19

Figure 16: Structure of [^{18}F] FEET **19**.[67]

However, radiopharmaceuticals like [^{18}F]-FES **18** and [^{18}F]-FEET **19** have a high liver and bowel uptake which can interfere with the detection of lesions in or near these organs. This leads to a background signal which makes it harder to identify metastases in these areas.[71, 72] Additionally, [^{18}F]-FES and [^{18}F]-FEET use fluorine-18, a radioactive isotope of fluorine which has a half-life of 110 minutes.[73] Hence, the molecule must be used relatively quickly after production, limiting its usefulness if longer transport times are required.

1.3.2 The 17th Position of a Functionalised Estradiol

Functionalising estradiol **16** requires considerations of where to append additional groups as the ligand binding domain of hERα has several key binding interactions with estradiol. Key to these interactions is a network of hydrogen bonds as well as Van Der Waal's forces. The main stabilising interactions involve protein residues Glu353, Arg394, Phe404 and His524 (Figure 17).[74]

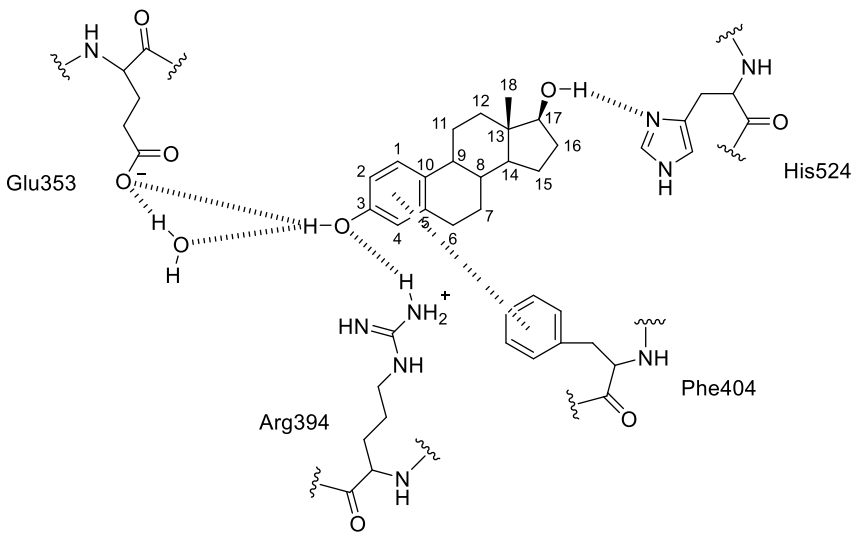

Figure 17: Key stabilising interactions with estradiol.[74]

Many previous reports have focused on functionalisation of the 17th position of the estradiol.[75-77] It has been shown that introducing bulky groups at this position does not inhibit binding to hERs,[76] and estradiol derivatives functionalised at this position retain their estrogenic properties and maintain their selectivity for hER. Hanson *et al*. investigated the effect of functionalising estradiol with phenylvinyl groups.[78] Introducing a phenyl group at C17 reduced binding affinity by only 4.0%, while the addition of a pyridine ring or a bipyridyl rhenium complex had no effects on binding affinity. Hence, the 17th position of estradiol is a common target for pharmaceutical development due to its ability to accommodate bulky functional groups without significantly impacting binding affinity.

1.4 Project Aims

The development of metal-based therapeutics continues to hold great promise due to their unique chemical reactivity and biological potency. However, the lack of selectivity remains a persistent challenge, and means that these agents often result in serious side effects. Strategies using click chemistry to functionalise cyclam-based ligands offer a way to address this issue by enabling the construction of selective chemical sensors and target-activated metal complexes (TAMCs). Incorporating ^{19}F-labelled triazoles into such systems is a potential way to enable real-time monitoring of metal coordination through sensitive NMR and imaging techniques. By functionalising at biologically validated sites-such as the 17th position of estradiol in agents that will target estrogen receptor-positive tissues, this approach offers a promising pathway toward next-generation metallodrugs that are both effective and precisely activated at their site of action.

The overall aim of this thesis is to develop and investigate cyclam-fluorotriazolyl derivates for sensing applications by exploiting the versatile metal-binding capability of cyclam and the synthetic simplicity of the CuAAC reaction to obtain target triazolyl derivatives.

Chapter Two describes the synthesis of the 5-fluorotriazolyl-cyclam ligand target (Figure 18) and its zinc complex. Previous studies have utilised ^{1}H and ^{2}H NMR to visualise triazole displacement from a metal-cyclam complex. Extending this approach, ^{19}F NMR offers more sensitive means of visualising triazole displacement from a metal-cyclam complex. The aim of the work described in this chapter is to develop a synthetic route to a fluorinated-triazole-cyclam complex utilising previously reported halogen exchange methods.

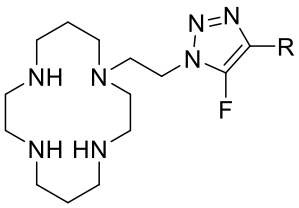

Figure 18: General structure of the ligand aimed to be synthesized in Chapter Two.

Chapter Three describes the ^{19}F NMR experiments to visualise the triazole displacement reaction, exploring the effectiveness of ^{19}F NMR as a means for visualising the triazole displacement by monitoring the fluorine environment of the 5-fluorotriazolyl-cyclam zinc complex obtained in Chapter Two. Chapter three also describes synthetic methods that can be used towards functionalisation of the 17th position of an estradiol to enable its incorporation in a suitable cyclam derivative. It has been previously shown that the binding affinity of estradiols is not significantly decreased by functionalising at the 17th position, and (separately) that a biotin-avidin binding event can trigger changes in metal coordination by a triazolyl-cyclam derivative. This idea can be further extended to monitor the estradiol-hER binding event (Figure 19).

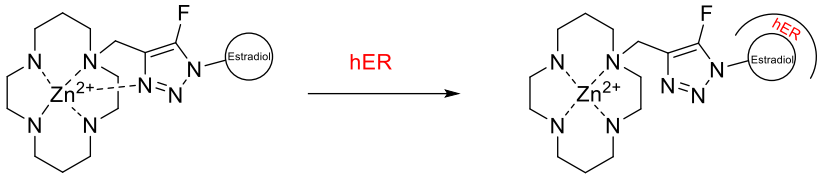

Figure 19: General scheme for estradiol-hER binding event.

Chapter 2 – Synthesis of 5-fluorotriazole-cyclam conjugates

2.1 Background

As previously discussed, metal complexes have become an increasingly important tool of modern medicine. Metal complexes have a wide range of uses including chemotherapeutics and imaging.[5, 8] However, their use is limited due to serious side effects in patients arising from a lack of selectivity.[3] Hence, target activated metal complexes (TAMCs) have become increasingly sought after.

Tamanini et al. first demonstrated target-activated metal complexes using a cyclam-triazole-biotin system, which was proposed to function via an 'allosteric scorpion mechanism' upon biotin binding to avidin, triggering a change in Cu^{2+} coordination geometry.[44] While this change was observed by EPR and ENDOR spectroscopy, poor signal-to-noise limited further analysis. Subsequent studies with a coumarin-labelled cyclam chemosensor showed that anion addition could modulate fluorescence by displacing the triazole ligand, as confirmed by ^{1}H NMR and electron spray ionisation mass spectroscopy (ESI LRMS).[45] Although ^{1}H NMR proved effective for studying these coordination changes, interference from protein signals led to the use of deuterated triazoles and ^{2}H NMR, however this presented a problem with regard to the concentration of proteins required for binding studies.[51]

We propose that ^{19}F NMR will provide a more sensitive method to study metal coordination geometry in cyclam complexes upon ligand binding coordination and decomplexation and further validate the target-activated "allosteric scorpion" system. This chapter describes the synthesis of 5-fluorotriazole-cyclam systems to enable ^{19}F NMR spectroscopic experiments to visualise binding events.

2.2 Proof of concept 5-fluorotriazole

To establish a baseline for optimizing conditions and exploring a viable synthetic route, a proof-of-concept (POC) molecule was synthesized. The benzyl-5-fluoro-triazole-phenyl compound **24**, previously reported in the literature, was selected as this POC target, and prepared as detailed in Scheme 2.1.[54]

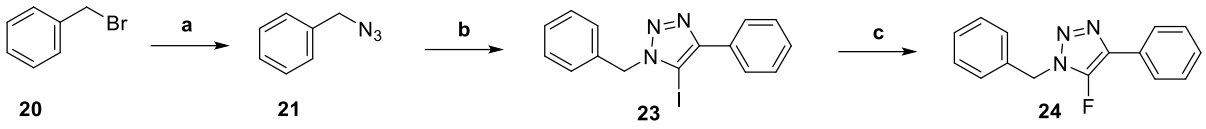

Scheme 2.1: Synthesis of POC compound **24**. **a.** NaN_3, acetone/H_2O (1:1), rt, 16h, 97%. **b.** 1-iodophenylacetylene **22**, Cu(I), TEA, THF, rt, 6h, ~40%; **c.** KF, MeCN/H_2O (1:1), 160°C, 15 min, ~50%.

For the synthesis of the benzyl-5-fluorotriazole-phenyl POC system, benzyl azide **21** was first obtained by stirring benzyl bromide **20** with sodium azide at room temperature in a mixture of acetone and water (1:1) to yield the desired product **21** in excellent yield (97%). Phenylacetylene was iodinated using N-iodomorpholine to yield 1-iodophenylacetylene **22** in excellent yield (93%). Using the CuAAC click conditions described in Hein *et al.*[55], 1-iodophenylacetylene **22** and benzyl azide **21** were combined to yield the corresponding 5-iodotriazole **23** in approximately 40% yield. To confirm whether fluorination by halogen exchange was possible, **23** was treated with ca. 5 equivalents of potassium fluoride in a mixture of acetonitrile and water (1:1) and reacted in a microwave reactor at 160°C for 15 minutes. ESI LRMS, ^{1}H NMR and ^{19}F NMR analyses all confirmed that the target compound **24** had been synthesized successfully in approximately 50% yield. The 5-iodotriazole product **23** and 5-fluorotriazole product **24** were not isolated nor fully characterized, as this was a POC. Instead, the synthesis of these products was confirmed spectrometrically using ESI LRMS and ^{1}H NMR.

The ^{19}F NMR spectrum of compound **24** (Figure 23) contained the key fluorotriazole peak at 152 ppm, consistent with previous reports of 5-fluorotriazole signals between -150 to -155 ppm.[57] Additionally, it demonstrated the high clarity of the fluorine peak in the absence of any other fluorine environments.

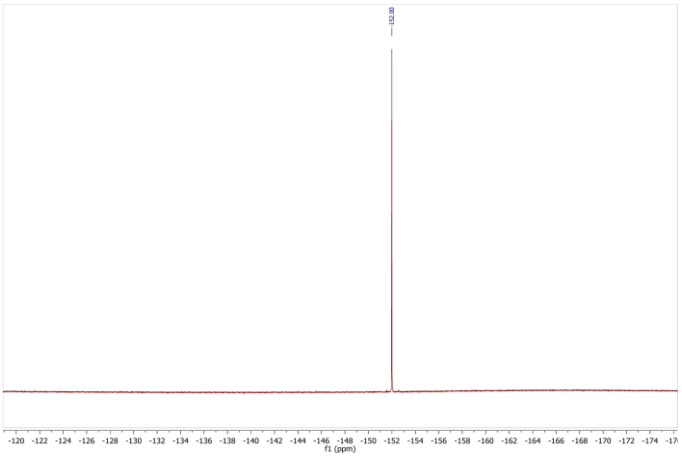

Figure 23: ^{19}F NMR of POC compound **24** in $CDCl_3$.

2.3 Synthesis of C4 cyclam-5-fluorotriazole-phenyl system

Armed with the ability to synthesize 5-fluorotriazoles from 5-iodotriazoles, the synthesis of the target cyclam-5-fluorotriazole-phenyl system (Chapter 1, Figure 18) was adapted from previously reported procedures developed in the Rutledge research group.[21, 51] The route proceeded via azidoethyl cyclam **28** as the key CuAAC click precursor. Wong *et al*. has previously demonstrated that molecules with C4 triazole connectivity exhibit a more pronounced shift in signal position for the triazolyl proton or deuteron upon triazole (de)complexation to the metal centre, relative to systems with N1 connectivity.[51] It was therefore anticipated that a similar effect would be observed for the fluorine signal, making the C4-substituted complex the priority target.

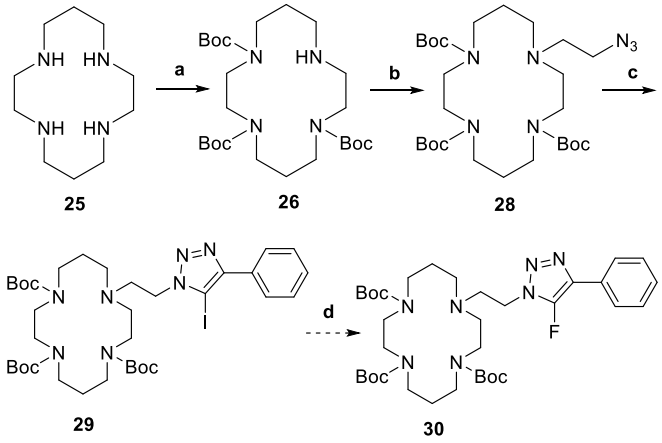

Scheme 2.2: Synthetic route to compound **30** containing C4 triazole connectivity. **a.** Boc_2O, TEA, DCM, 0°C to rt, 36h, 70% **b.** 2-azidoethyl toluenesulfonate **27**, NaI, K_2CO_3, MeCN, reflux, 48h, 88%; **b.** 1-iodo-phenylacetylene **22**, Cu(I), TEA, THF, rt, 6h, 46%; **d.** KF, MeCN/H_2O (1:1), 160°C, 15 min, not isolated.

For the synthesis of the C4 complex containing the phenyl pendant group connected via the 5 -fluoro-triazole, stoichiometric addition of 3 equivalents of di-*tert*-butyl dicarbonate to cyclam **25** afforded the tri-Boc protected cyclam **26** as the major product in good yield (70%). The di- and tetra-Boc protected by-products were easily removed by flash column chromatography. 2-Azidoethyl toluenesulfonate **27** was obtained by refluxing 2-bromoethanol with sodium azide in H_2O and then reacting the 2-azidoethanol with toluenesulfonyl chloride in DCM at room temperature in moderate yield (62%). Adapting previously reported procedures, 2-azidoethyl toluenesulfonate **27** was used to alkylate tri-Boc-cyclam to give azidoethyl-cyclam derivative **28** in excellent yield (88%).[51] The addition of 5 equivalents of sodium iodide significantly

increased the yield (from 28% to 88%) by enabling a one-pot, two-step synthesis via the alkyl iodide intermediate. In this process, the tosylate group undergoes an S_N2 Finkelstein-type reaction with sodium iodide, where the tosylate is displaced by iodide. As iodide is a superior leaving group, the subsequent nucleophilic substitution by the cyclam nitrogen proceeds more efficiently. As the alkylation procedure often caused low yield and the azide starting material **27** was not recovered, five equivalents of NaI were employed to match the excess of **27** used in previous literature, thereby improving reaction efficiency.[20]

Using the CuAAC conditions previously described, the azidoethyl-cyclam **28** was reacted with 1-iodo-phenylacetylene **22** to afford the Boc-protected-5-iodotriazole system **29** in moderate yield (46%).

The Boc-protected-5-iodotriazole product **29** was subjected to the halogen exchange conditions used with the POC system, however minimal conversion to the desired 5-fluorotriazole product **30** was observed. Trace amounts of the desired product were observed using ^{19}F NMR (Figure 24), although these peaks were relatively weak compared to the strong fluorine peak observed in the case of POC compound **24**. LRMS analysis confirmed the presence of the desired 5-fluorotriazole product **30** (Figure 25), revealing a small peak at *m/z* 712.42, corresponding to $[M + Na]^+$ for compound **30**, as well as a peak at 820.28 ($[M + Na]^+$), for starting material **29**. Subjecting the 5-iodotriazole precursor to higher equivalents of fluoride nucleophile (KF) led to the decomposition of the starting material. Utilising other fluoride nucleophiles (KHF_2 and AgF), led only to recovery of the starting material **29**.

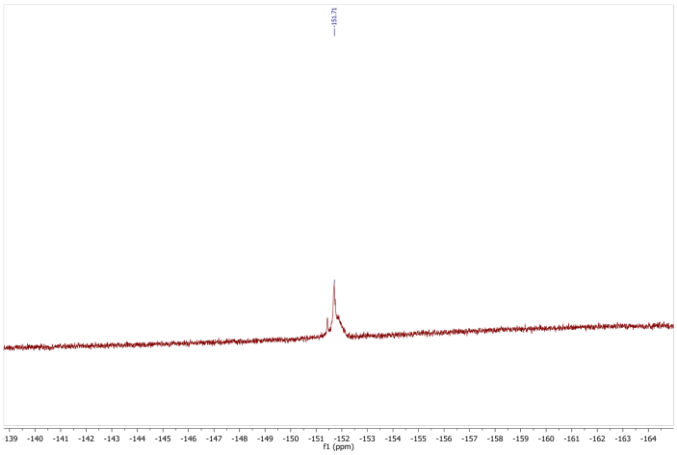

Figure 23: ^{19}F NMR ($CDCl_3$) of **30**.

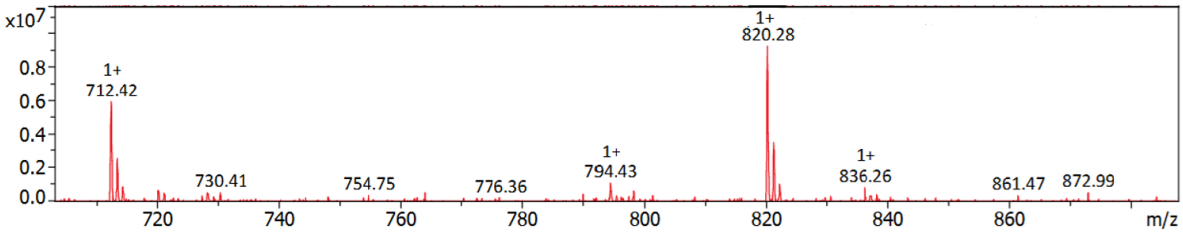

Figure 24: MS analysis of reaction mixture **d** (Scheme 2.2) with peaks corresponding to **29** (820.28) and **30** (712.42).

The low conversion of **29** meant that, the 5-fluorotriazole-cyclam compound **30** was not isolated. It is possible that the bulky Boc groups present on the cyclam inhibit the substitution of the iodine atom by the fluorine atom. The halogen exchange reaction proceeds via an S_NAr type reaction and, as explored by Agami *et al*., N-Boc groups are resistant to many nucleophilic reagents making them poorly reactive in S_NAr type reactions.[79] This structural inertness can create a 'steric shield' around reactive centres, significantly hindering nucleophiles from achieving the necessary nucleophilic attack for substitution. The presence of 3 N-Boc groups around the cyclam core in compound **29** likely prevents the fluoride nucleophile from effectively approaching the 5-iodotriazole, leading to lower conversion rates. To circumvent this issue, an alternative reaction sequence was formulated in which the halogen exchange reaction can occur before alkylation of tri-Boc-cyclam.

To retain the C4 connectivity known to enhance sensitivity, 2-azidoethyl toluenesulfonate **27** was subjected to the CuAAC conditions previously described with 1-iodophenylacetylene **22**. The reaction yielded no desired product, and the starting materials could not be recovered. The presence of Cu(I) in the reaction may have contributed to this outcome. Cu(I) is known to participate in copper-catalyzed reductive cross-coupling reactions involving alkyl tosylates, suggesting that it may have interacted with the tosylate leaving group, resulting in its displacement and the formation of unwanted side products.[80] Given the difficulties encountered in pursuit of C4 connectivity, an alternative route to synthesize N1 complexes containing a benzyl pendant group connected via the 5-fluorotriazole was investigated.

2.4 Synthesis of N1 cyclam-5-fluorotriazole-phenyl system

The route to N1 connected cyclam-5-fluorotriazole metal complex **37** was adapted from published procedures, proceeding via the iodinated alkyne **32** as the key CuAAC click precursor.[51, 55]

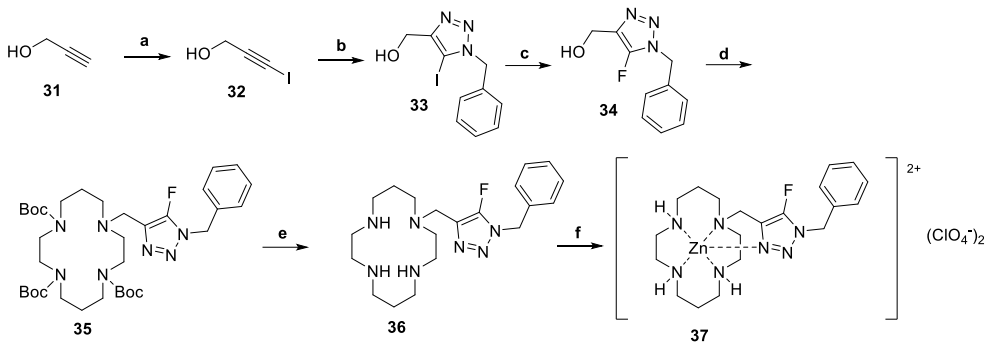

Scheme 2.2: Synthesis of the zinc complex **37** incorporating N1 triazole connectivity. **a.** I_2, NaOH, MeOH, 0°C to rt, 16h, 48%; **b.** Benzyl azide **21**, Cu(I), TEA, THF, rt, 6h, 48%; **c.** KF, MeCN/H_2O (1:1), 160°C, 15 min, 69%; **d.** i) TEA, MsCl, rt, 16h, ii) tri-Boc-cyclam **26**, NaI, K_2CO_3, MeCN, reflux, 48h, 72%; **e.** i) HCl, dioxane, rt, 16 h, ii) Ambersep® 900 hydroxide form resin, MeOH, rt, 10 min, 98%; **f.** $Zn(ClO_4)_2 \cdot 6H_2O$, EtOH, rt, 16 h, 46%.

For the synthesis of the N1 complex with one carbon atom between the cyclam and the triazole (Scheme 2.2), 2-propyn-1-ol **31** was iodinated with iodine and sodium hydroxide to afford 3-iodoprop-2-yn-1-ol **32** in moderate yield (48%). Using the CuAAC click conditions previously described, the iodoalkyne **32** was clicked with benzyl azide **21** to afford the desired 5-iodotriazole **33** in moderate yield (48%). Using the halogen exchange reaction conditions previously reported, KF was reacted with **33** and a good conversion to the desired 5-fluorotriazole **34** was observed (69%). By first mesylating this fluoroalcohol and using alkylation conditions adapted from those shown in Scheme 2.2, a one-pot two step synthesis involving the 5-fluorotriazole **34** was used to alkylate the tri-Boc-cyclam **26** to give the desired Boc-protected cyclam-5-fluorotriazole ligand **35** in good yield (72%). HCl-mediated deprotection gave the HCl salt of **35** which was neutralised with Ambersep ® 900 hydroxide form resin in methanol to give the desired cyclam-5-fluorotriazole ligand **36** in quantitative yield. Adapting the previously reported method,[51] stirring with zinc perchlorate at room temperature overnight followed by filtration afforded the metal complex **37** in moderate yield (46%). Zinc complexation was confirmed by the presence of the expected Zn and Cl isotopic distributions in the ESI-LRMS spectrum.

2.5 The 'n = 2' route to the cyclam-5-fluorotriazole-phenyl system

Furthermore, to explore the effect of the distance of the 5-fluorotriazole from the complexed macrocycle, a similar route was used to generate an alternative system incorporating a 2-carbon spacer between the cyclam nitrogen and the triazole.

Synthesis of this alternative N1 connected cyclam-5-fluorotriazole metal complex **47** with two carbon atoms between the cyclam and triazole was adapted from published procedures,[51, 55] proceeding via the iodinated alkyne **39** as the CuAAC click precursor.

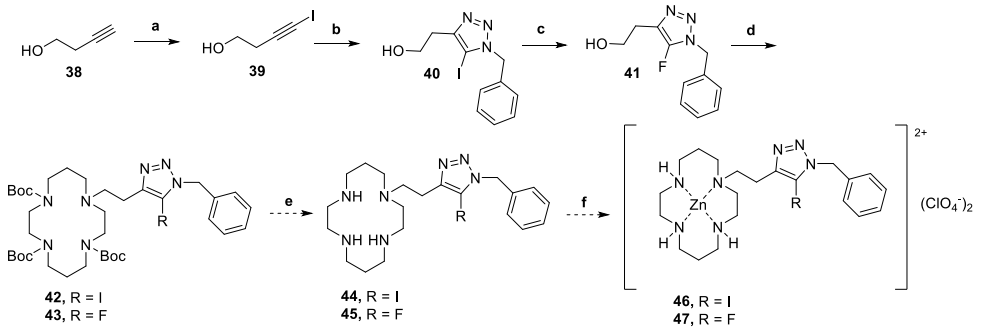

Scheme 2.3: Synthetic route to the complex mixture **46**/**47** containing N1 triazole connectivity. **a.** I_2, NaOH, MeOH, 0°C to rt, 16h, 56%; **b.** Benzyl azide **21**, Cu(I), TEA, THF, rt, 6h, 47%; **c.** KF, MeCN/H_2O (1:1), 160°C, 15 min, 5%; **d.** i) TEA, MsCl, rt, 16h, ii) tri-Boc-cyclam **26**, NaI, K_2CO_3, MeCN, reflux, 48h; **e.** i) HCl, dioxane, rt, 16 h, ii) Ambersep® 900 hydroxide form resin, MeOH, rt, 10 min; **f.** $Zn(ClO_4)_2 \cdot 6H_2O$, EtOH, rt, 16 h.

For the synthesis of complex **46**/**47** (Scheme 2.3), 3-butyn-1-ol **37** was iodinated using procedures adapted from that shown in Scheme 2.2 to afford the desired 4-iodobut-3-yn-1-ol **39** in moderate yield (56%). Using the CuAAC click conditions adapted from that shown in Scheme 2.1, the iodinated alkyne **39** and benzyl azide **21** were clicked to afford the 5-iodotriazole **40** in moderate yield (47%). 5-Iodotriazole **40** was converted to 5-fluorotriazole **41** in poor yield (5%) using the potassium fluoride methodology detailed earlier. Unlike the 'n = 1' route, conversion to the fluoro-derivative was incomplete and quantities of the iodide starting material were still present in the product mixture. The starting material **40** and desired product **41** possess very similar polarity, making separation by flash column chromatography challenging. Adding more equivalents of KF and increasing the reaction time did not lead to higher conversion of iodo-triazole **40** to fluoro-triazole **41**. As a result, liquid chromatography mass spectroscopy (LC-MS) and reversed-phase liquid chromatography were employed to isolate the target compound **41**, reducing yields. This strategy afforded only limited quantity of **41** and meant that it was not viable to continue the route using the purified compound. Furthermore, large-scale use of benzyl azide was avoided for safety reasons. As a result, the mixture of compounds **40** and **41** was employed to facilitate progression through the synthetic pathway and enable the isolation of downstream products. Adapting the mesylation/alkylation procedure previously discussed, the mixture of 5-fluorotriazole **41** and 5-iodotriazole **40** was used to alkylate tri-Boc-cyclam **26** to give the desired 'n=2' Boc-protected cyclam-5-fluorotriazole **43** as a mixture (2:1) with the Boc-protected cyclam 5-iodotriazole **42**. Attempts

to further purify compound **43** were unsuccessful. However, based on the data collected from the fluorinated molecule **37**, it was concluded that, despite being part of a mixture, the sample could still offer valuable insights into the effect of carbon chain length on monitoring triazole displacement. HCl-mediated Boc deprotection gave the HCl salts of **44** and **45** in a mixture which was neutralized with Ambersep ® 900 hydroxide form resin in methanol to give the desired 'n=2' cyclam-5-fluorotriazole ligand **45** as a mixture (7:3) with the cyclam-5-iodotriazole impurity **44**. Due to the similar polarities of the iodinated (**44**) and fluorinated (**45**) triazole derivates, chromatographic separation proved challenging. The difficulties encountered in purification are likely responsible for the variations observed in the relative proportions of the two compounds at different stages of the synthesis.

Using previously reported methods, stirring the cyclam macrocycle with zinc perchlorate at room temperature overnight followed by filtration afforded the metal complex **47** and the 5-iodotriazole metal complex **46** as a mixture. Relative abundances of the 5-iodotriazole and 5-fluorotriazole complexes could not be determined due to multiple overlapping signals in the ^{1}H NMR and the ^{13}C NMR spectra as a result of the mixture.

2.5 Conformational isomers of cyclam

Qualitative studies first performed by Bosnich *et al*. described five isomers of simple metal complexes of cyclam.[81] These five isomers (*trans-I – trans-V,* Figure 25) differ in the shape adopted by the macrocycle, the orientation of the pendant group atoms attached to each N atom, and their energetic stability, which contributes to their relative abundance in solution.[82]

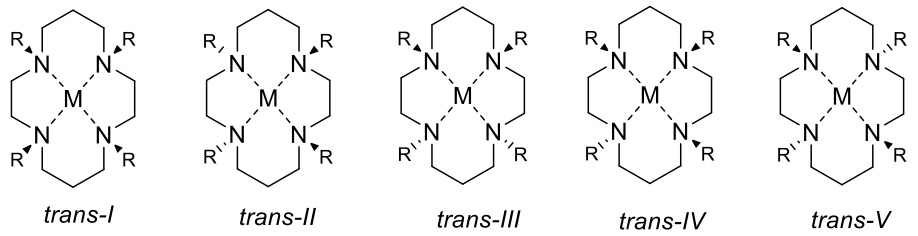

Figure 25: The five known isomers of metal complexes of cyclam.

Bosnich *et al*. confirmed that if the number of nitrogen substituents is two or lower, the *trans-III* conformation is usually the most stable, with the hydrogen/substituents bound to nitrogen atoms N1 and N11 of the cyclam macrocycle pointing to the same direction/face of the macrocycle, whereas hydrogen atoms/substituents on nitrogen atoms N4 and N8 both point in the opposite direction.[81] Liang *et al*. previously investigated the relative abundance of

perchlorate complexes of Zn^{2+} cyclam using ^{1}H NMR spectroscopy.[83] Their study revealed that the distribution of cyclam configurational isomers varies based on factors including length of time in solution and pH. Initially (t = 0), the predominant species was the *trans*-III configuration, which constituted approximately 90% of the isomer population. After 10 hours, the abundance of *trans*-V increased significantly, and *trans*-I showed a slight increase, indicating an equilibrium distribution of approximately 43:42:15 for *trans*-III:*trans*-V:*trans*-I (with neither the *trans-II* nor *trans-IV* isomers present at detectable levels). Liang *et al*. also studied the effect of temperature, observing changes (up to -4.5 parts-per-billion per Kelvin ($ppbK^{-1}$)) in the chemical shifts of *trans-III* and *trans-I* isomers whilst the *trans-V* isomers chemical had a smaller change (-0.8 $ppbK^{-1}$). As the temperature is increased both the chemical shifts of the isomers change as well as their relative abundance in solution. They concluded that for perchlorate metal complexes such as **37** and **47**, *trans-III* is the predominant configuration, with *trans-V* and *trans-I* present as minor forms. Complementary work by Lelong *et al*. explored the influence of solvent on isomer distribution, showing that different solvents can preferentially stabilize particular coordination geometries through hydrogen bonding or weak coordination interactions.[84] Furthermore, cyclam complexes containing fluorine atoms such as the copper complex of **15** (see Section 1.2.5) have been previously observed to have multiple peaks in their ^{19}F NMR spectra due to conformational isomers.[60]

For complexes **37** and **47**, similar trends are expected as the position of the pendant arm would be significantly affected by the different geometries it can adopt in relation to the cyclam core as well as the different geometries of the secondary amine hydrogens. Spectroscopic techniques such as ^{19}F NMR (Figure 26) and ^{1}H NMR (Figure 27) confirm the presence of configurational isomers in these systems.

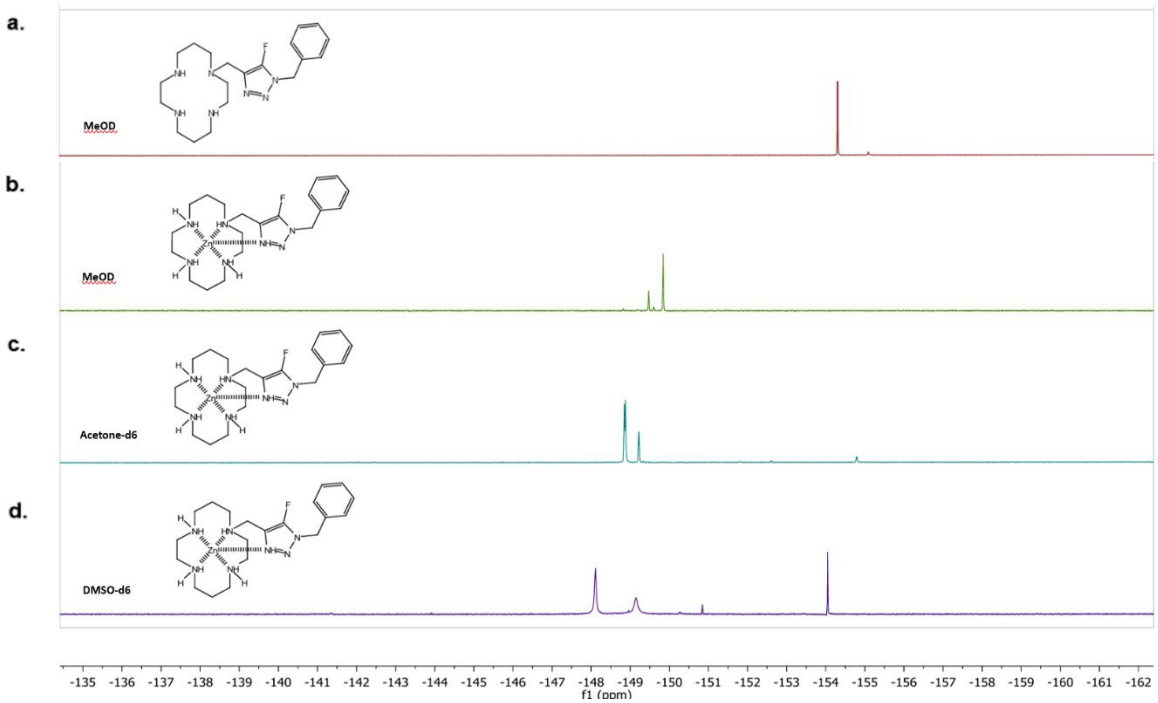

Figure 26: ^{19}F NMR spectra of compounds **36** (triazolyl-cyclam) and **37**.(zinc-cyclam complex) **a.** ^{19}F NMR peak of 5-fluorotriazolyl-cyclam compound **36**; **b.** ^{19}F NMR peaks of zinc complex **37** in MeOD. **c.** ^{19}F NMR peaks of zinc complex **37** in acetone-d6; **d.** ^{19}F NMR peaks of zinc complex **37** in DMSO-d6.

The spectrum **36** in MeOD (Figure 26a) shows the ^{19}F fluorine NMR spectrum of the uncomplexed 5-fluorotriazolyl-cyclam **36** which has only a main single fluorine peak. Upon complexation with zinc, the cyclam structure of **37** becomes rigid and conformationally locked by amine coordination to the metal, so the isomers become apparent, with two ^{19}F signals evident in the spectrum. As previously explored by Lelong *et al*., different solvents lead to different relative abundance of isomers in solution.[84] The spectrum of **37** in MeOD (Figure 26b) shows two main peaks, likely corresponding to the *trans-III and trans-V* isomers with the *trans-III* isomer presumed to be the most abundant on the basis of the literature precedent. The spectrum of **37** in acetone-d6 (Figure 26c) also shows two main peaks, expected to be the *trans-III* and *trans-V* isomers. Similarly, the spectrum of **37** in DMSO-d6 (Figure 26d) shows three main peaks, based on relative abundance, the signals might be tentatively assigned to be the *trans-III* (154 ppm), *trans-V* (148 ppm) and the *trans-I* (149 ppm) isomers. Minor peaks, most noticeable in Figure 26 **b** and **d** possibly represent the less common isomers. The variation in signal distribution and relative abundance across the different solvent systems supports the presence of multiple configurational isomers in solution.

To further investigate whether the observation of multiple fluorine peaks in the spectra of **37** do in fact arise due to isomeric factors, variable temperature ^{1}H NMR experiments were conducted with the zinc complex **37** (Figure 27). As previously explored by Liang *et al.* changing the temperature of the solution results in minor changes in the chemical shifts of the *trans-III* and *trans-I* isomers.[83] By increasing the temperature and observing relevant changes in the chemical shifts, it may be possible to determine whether isomers are indeed present.[85] Figure 27 shows variable-temperature ^{1}H NMR spectra of **37** in the temperature range 300 to 340K highlighting the CH_2 peak from the benzyl pendant group. This peak was chosen as it remains unobstructed upon zinc complexation.

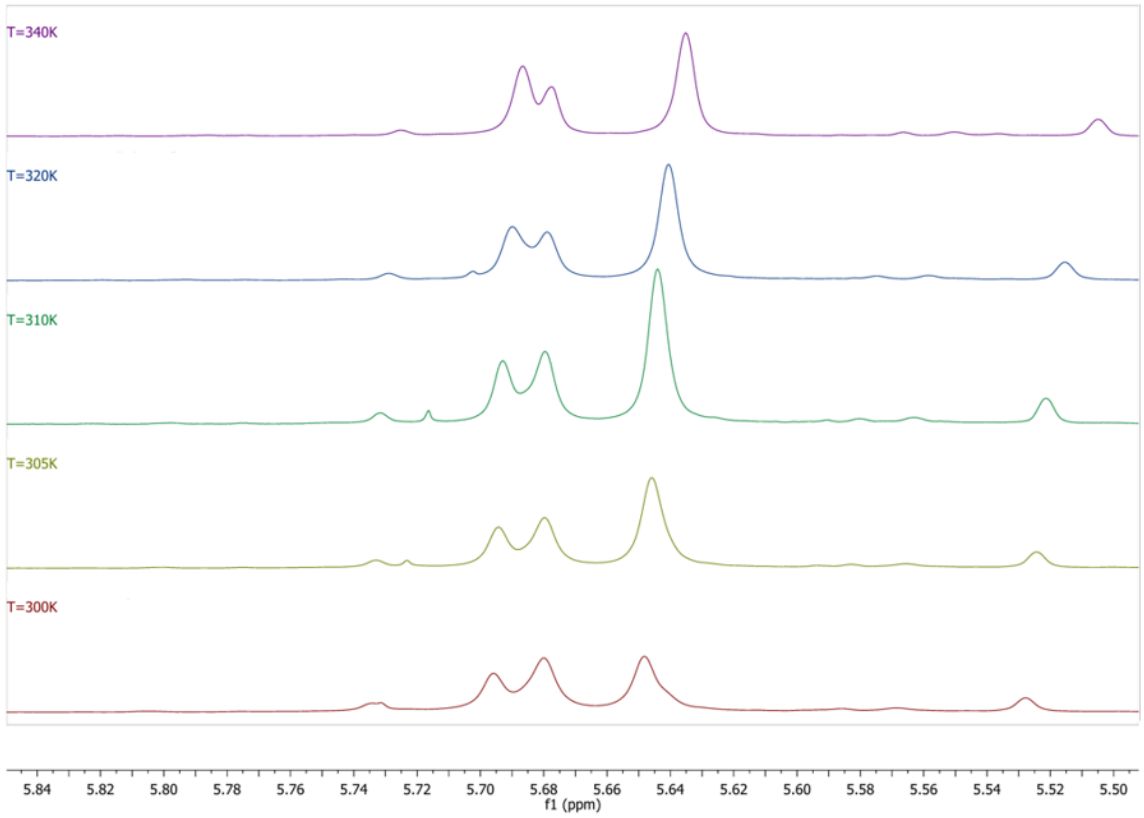

Figure 27: ^{1}H NMR spectra of the benzyl CH_2 of **37** at different temperatures (300 – 340K).

The presence of multiplet peaks in the ^{1}H NMR for these protons highlights that there are indeed multiple proton environments, consistent with the presence of different compound isomers in solution. Upon increasing the temperature from 300 K to 340 K, the lowest-field of these peaks shifts from 5.6959 ppm to 5.6866 ppm ($\Delta\delta$ = -0.0093 ppm, -0.25 ppbK^{-1}), the highest-field of these peaks shifts from 5.6482 ppm to 5.6352 ppm ($\Delta\delta$ = -0.013 ppm, -0.33 ppbK^{-1}), and the central peak shifts only slightly from 5.6800 ppm to 5.6775 ppm ($\Delta\delta$ = –0.0025 ppm, –0.06 ppbK^{-1}). These values are smaller than those reported by Liang *et al.* in

their investigations, likely because the CH_2 signals in this system originate from positions further from the cyclam core.[83] However, the relative ratios of chemical shift change (~1:6) are consistent with the observations made by Liang *et al*.. Based on both the magnitude of the shifts and the relative peak intensities, it is possible that the highest-field and lowest-field of these peaks might tentatively be assigned to *trans-III* and *trans-I* isomers respectively, with the less responsive central peak corresponding to the *trans-V* isomer. However, further investigation is required to confirm this hypothesis.

Confirming whether zinc complexes **46**/**47** exhibit similar isomeric behaviour proved to be difficult due to the presence of several peaks in the ^{19}F NMR of the complexed cyclam species. This may be attributed to the longer carbon chain in complex **46**/**47** which increases the distance between the triazole nitrogen donor and the zinc centre and is further discussed in Section 3.2.3. The uncomplexed cyclam ligand can also adopt different configurational isomers,[81] although these are typically not distinguishable by ^{1}H NMR spectroscopy. In its uncoordinated form, cyclam is flexible and can rapidly convert in solution, so NMR spectra typically show averaged signals and hence confirming the presence of configurational isomers is challenging. However, due to the fact that the large 5-fluorotriazole ligand is attached on the cyclam, steric bias is introduced, slowing down conformational interconversion, potentially making individual conformers observable as this also causes the macrocycle to favour certain confirmations over others.[86] Figure 28 shows the presence of multiple peaks in the ^{19}F NMR of free ligand **44**/**45.**

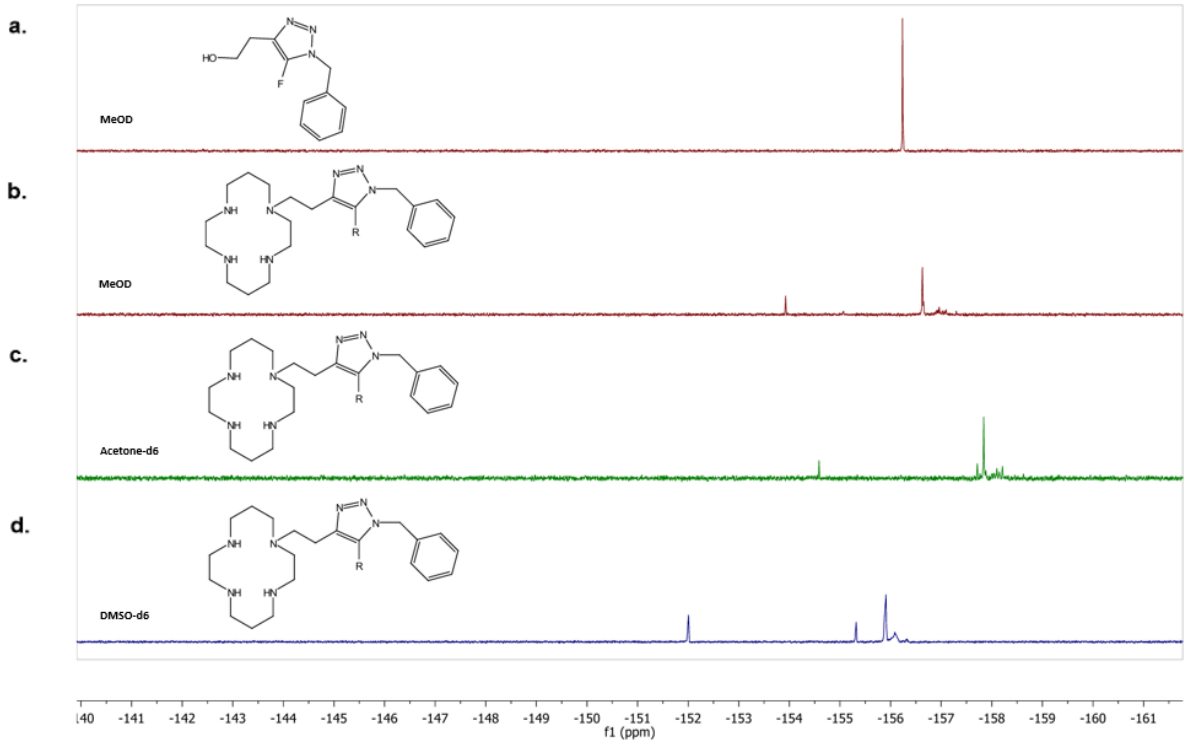

Figure 28: ^{19}F NMR spectra of compounds **41** and **44**/**45**. **a.** ^{19}F NMR spectrum of **41** in MeOD. **b.** ^{19}F NMR spectrum of **44**/**45** in MeOD. **c.** ^{19}F NMR spectrum of **44**/**45** in acetone-d6. **d.** ^{19}F NMR spectrum of **44**/**45** in DMSO-d6.

Although multiple peaks are present in the uncomplex cyclam mixture **44/45** there is no robust evidence to confirm that the relative abundance of isomers in solution changes as the solvent is changed. Due to the inability to isolate compound **44**/**45** or complex **46/47**, their ^{1}H NMR spectra are inconclusive with respect to configurational isomerism, as extensive peak overlap prevents clear differentiation of individual species in solution. However, similar isomeric factors for complex **46/47** are expected as confirmed by complex **37.**

2.6 Conclusion

The 5-fluoro cyclam conjugate **36** featuring a N1-substituted triazole linkage has been successfully synthesized. The alternative 5-fluoro cyclam conjugates **45** and **30** featuring N1 and C4-substituted triazole linkages respectively have been synthesized but not isolated in pure form. Zinc complexes of the N1-substituted 5-fluorotriazole-cyclam conjugates **37** and **47** were also prepared and characterized using a range of analytical techniques. The presence of isomers of complex **37** and ligand mixture **44**/**45** was investigated using both ^{1}H NMR and ^{19}F NMR techniques.

Chapter 3 – ^{19}F NMR Visualisation of Triazole Displacement

3.1 Background

^{19}F NMR spectroscopy offers greater sensitivity and a broader dynamic range than more commonly used ^{1}H and ^{2}H NMR techniques. Although its sensitivity is approximately 83% that of ^{1}H NMR, ^{19}F NMR benefits from a chemical shift range that is 50 times wider, 100% natural isotopic abundance, and minimal background signals due to the rarity of fluorine in naturally occurring biomolecules.[87]

With a large and growing demand for sensitive diagnostic methods to monitor biological interactions, ^{19}F NMR spectroscopy offers a simple and synthetically available way to monitor these. Previous work in the Rutledge group has employed ^{1}H NMR, MS, and ^{2}H NMR to demonstrate that a pendant triazole ligand, which contributes to the stabilization of zinc 'scorpionand' cyclam complexes, can be displaced from the metal by the addition of trisodium citrate or piperidine in 100-fold excess.[51] The resulting upfield shift of the key triazole signal is consistent with displacement of the triazole-phenyl pendant group from the Lewis acidic Zn^{2+}.

We envisage that the fluorine-containing zinc complexes **37** and **47** will undergo similar displacement upon the addition of anions, and that the resulting change in metal coordination geometry in these cyclam conjugates can be monitored by ^{19}F NMR spectroscopy. This technique offers several key advantages over ^{1}H and ^{2}H NMR, discussed above. These benefits open the prospect of ^{19}F NMR spectroscopy being a clearer and more sensitive method for observing triazole displacement from the metal.

3.2 ^{19}F NMR Investigations

3.2.1 ^{19}F NMR fluorine reference

Deuterated solvents are commonly used in NMR experiments to allow the instrument to lock onto an abundant nucleus and provide a stable reference point, while also minimizing interference from the hydrogen nuclei in the solvent.[88] In the absence of a fluorinated NMR solvent, there is no intrinsic reference signal for ^{19}F NMR. Although NMR instruments are able

to indirectly reference based on a ^{1}H NMR solvent lock, for precise readings and comparisons between spectra, a reference ^{19}F signal is required. Hence, NMR investigations were performed in the presence of fluorobenzene, which returns a strong, clear signal at -115.42 ppm in deuteromethanol (CD_3OD).[89] This reference additive provides a baseline for the ^{19}F NMR experiments and allows easier tracking of the 5-fluorotriazole peak of interest. Previous reports have shown that the fluorine signal of 5-fluorotriazoles occurs in the -150 to -155 ppm range, well clear of the fluorobenzene signal.[54] Fluorobenzene is also relatively inert and does not react with any species present in our sample solutions. CD_3OD was chosen as the solvent for these experiments as all of the free ligands, metal complexes and triazole displacement agents required for the ^{19}F NMR investigations are readily soluble in this solvent.

3.2.2 ^{19}F NMR experiments with 'n = 1' ligand

To establish a baseline for the analysis and changes in the position of the fluorotriazole signal, free ligand **36** was isolated and a quantitative amount (0.1 mL) of fluorobenzene was added as a reference. The ^{19}F NMR spectrum of compound **36** (Figure 29) gave a baseline for the subsequent complexation and triazole displacement experiments. The fluorotriazole peak was observed as a singlet at -154.5 ppm.

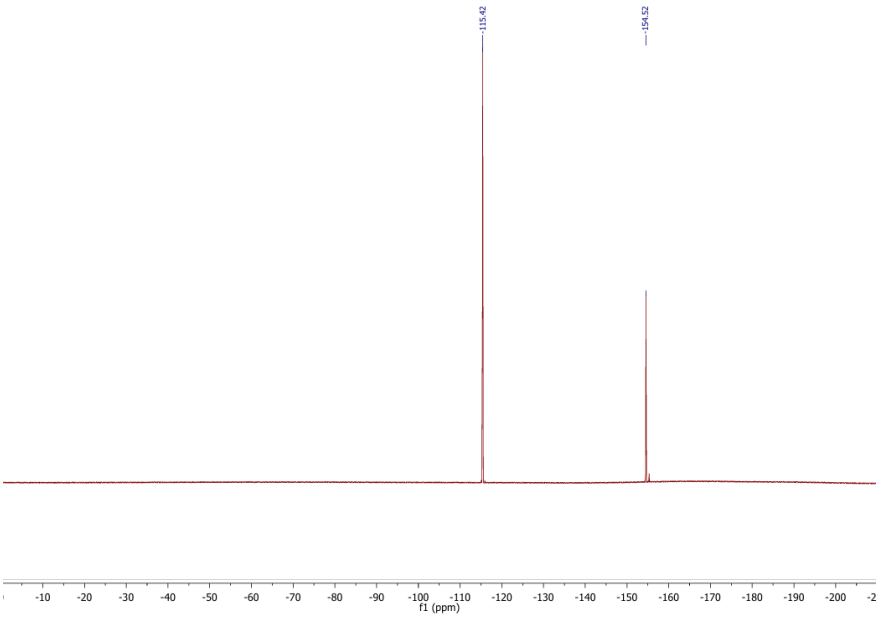

Figure 29: ^{19}F NMR spectrum of compound **36** in CD_3OD with fluorobenzene as reference.

Upon complexation of free ligand **36** with zinc perchlorate to form zinc complex **37**, the fluoro-triazole peak moved downfield to -149.9 ppm, a change of 4.6 ppm (Figure 30). This major peak is accompanied by a second, minor peak at -149.5 ppm, presumably the result of

variability in cyclam configuration around the metal centre in the complex, as discussed in Chapter 2. To displace the triazole ligand from the metal centre, piperidine was chosen as it had been previously utilised for displacement of the zinc ion.[51] After the addition of 100 equivalents of piperidine, the fluoro-triazole peak has moved upfield to -156.4 ppm, a change of 6.5 ppm (Figure 30).

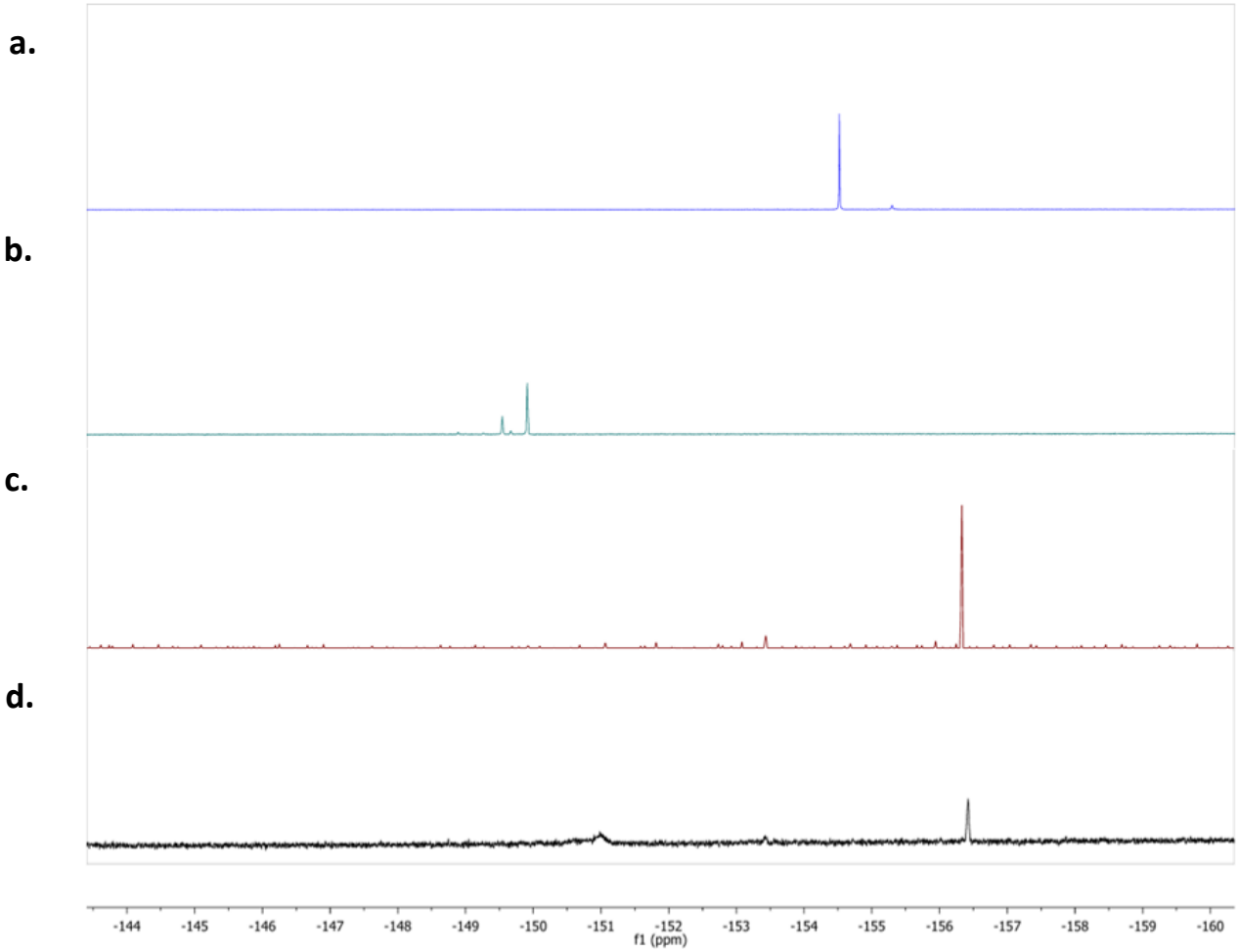

Figure 30: Using ^{19}F NMR spectroscopy to visualize triazole displacement with piperidine. (Referenced to fluorobenzene, seen at -115.4 ppm). **a.** free ligand **36**; **b.** zinc complex **37**; **c.** zinc complex **37** + 0.3 mL piperidine**; d.** free ligand **36** + piperidine (100 equiv.).

The apparent ~2 ppm difference in the position of the fluorine signal in the sample of complex **37** + piperidine relative to the ppm value of the free ligand **36**, is due to the presence of piperidine (100 equiv.) in solution. To confirm this, the same volumetric amount (0.3 mL) of piperidine was added to the NMR solution of free ligand **36**: The resulting ^{19}F NMR spectrum (Figure 30 d) confirmed these suspicions with the main fluorine peak of **36** shifting upfield to -156.1 ppm upon addition of 0.3 mL of piperidine.

To confirm that the metal ion remained coordinated to the macrocycle, MS experiments were run on the sample of complex **37** + piperidine (100 equiv.). Zinc and chlorine (from the perchlorate counter ion) display characteristic isotopic patterns: zinc has five stable isotopes ^{64}Zn, ^{66}Zn, ^{67}Zn, ^{68}Zn, and ^{70}Zn with average natural abundances of 49%, 28%, 4%, 19% and <1% respectively;[90] chlorine has two stable isotopes ^{35}Cl and ^{37}Cl with relative natural abundances of 76% and 24%.[91] ESI MS data of samples that contain perchlorates can be difficult to analyse due to the range of perchlorate adducts that form, adding complexity to the mass spectrum. Hence, MALDI-TOF MS was utilised to determine whether the zinc ion remains coordinated to the macrocycle after triazole displacement (Figure 31).

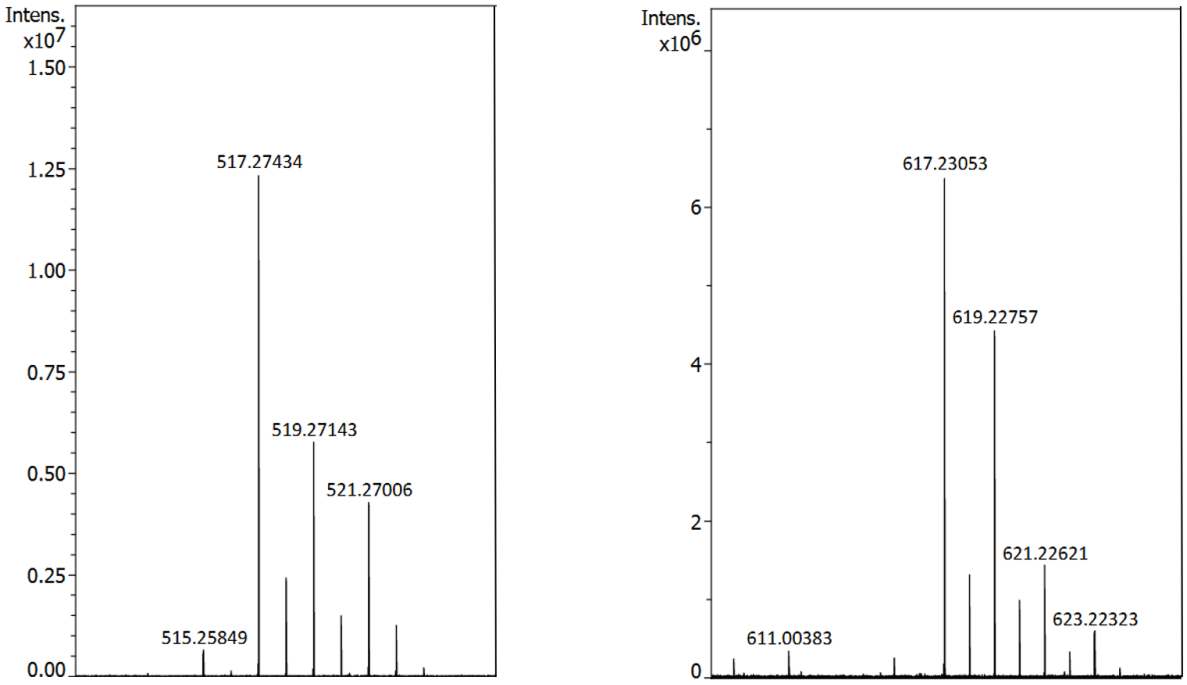

Figure 31. Expansion of peaks: MALDI-TOF analysis of complex **37** + 100 equiv. piperidine (α-CCA matrix).

As explored previously, mass spectra from the complex + piperidine sample do not provide confirmatory evidence for a **37**:piperidine complex.[51] However, the isotopic pattern can be used to verify whether zinc remains coordinated to the macrocycle. By inspecting the isotopic pattern of the peak at 517 *m/z,* the peak intensities reflect natural abundance probabilities of zinc; the closely spaced isotopic pattern and isotopic spread over 6 mass units also confirms that zinc remains coordinated to the macrocycle. The peak at *m/z* 517 likely corresponds to loss of two perchlorates and HF ([piperidine:zinc complex **37** – $2ClO_4$ – HF - H]$^+$). HF elimination is a well-established gas-phase fragmentation for fluorinated aromatics and arises via unimolecular elimination pathways (for example, via a "ring-walk" in fluorophenols).[92] Although the ring-walk mechanism is unlikely for 1,2,3-triazoles because of the heteroatom-

rich ring, analogous heteroatom-assisted HF-elimination or direct C-F bond cleavage processes are mechanistically plausible and have been observed for other fluorinated heterocycles under ionising conditions.[93] Without further MS studies, the exact nature of this species cannot be determined, however isotopic patterns provide confirmatory evidence of the presence of zinc.

Previous work by Wong *et al*. demonstrated that only peaks corresponding to the zinc-cyclam species having lost one or both its perchlorate counterions appear in the MALDI-TOF analysis of zinc complexes.[51] This supports the assignment of the peak at *m/z* 517 to a species that has lost two perchlorate ions, and the peak at *m/z* 617 to a species with the loss of a single perchlorate ([piperidine:zinc complex **37** – ClO_4 – HF]$^+$), as it is 100 Da heavier. The isotopic pattern of the *m/z* 617 peak is consistent with the natural abundances of zinc and chlorine, further supporting that zinc remains coordinated to the macrocycle. However, as previously mentioned, the exact nature of these species remains to be fully determined.[51] The isotopic distribution, together with the ^{19}F NMR spectra, confirms that zinc remains coordinated to the macrocycle and that the presence of piperidine influences triazole displacement from the Zn^{2+}centre.

3.2.3 ^{19}F NMR experiments with 'n = 2' ligand

Although the second fluorotriazole target could not be isolated in fully pure form (with the iodinated precursor a minor contaminant), the mixture of complexes **46**/**47** could nonetheless provide useful ^{19}F NMR data on the effect of lengthening the carbon chain as impurity **46** does not contain fluorine. For the 'n = 2' ligand, the same procedures and NMR experiments as described for the 'n = 1' ligand were utilised. Free ligand **44**/**45** + 100 equiv. (~ 0.3 mL) piperidine was analysed by ^{19}F NMR spectroscopy with a fluorobenzene reference. The ^{19}F NMR spectrum (Figure 32) shows the reference point for the subsequent zinc complexation and triazole displacement reactions. The main triazole peak is observed at -157.2 ppm.

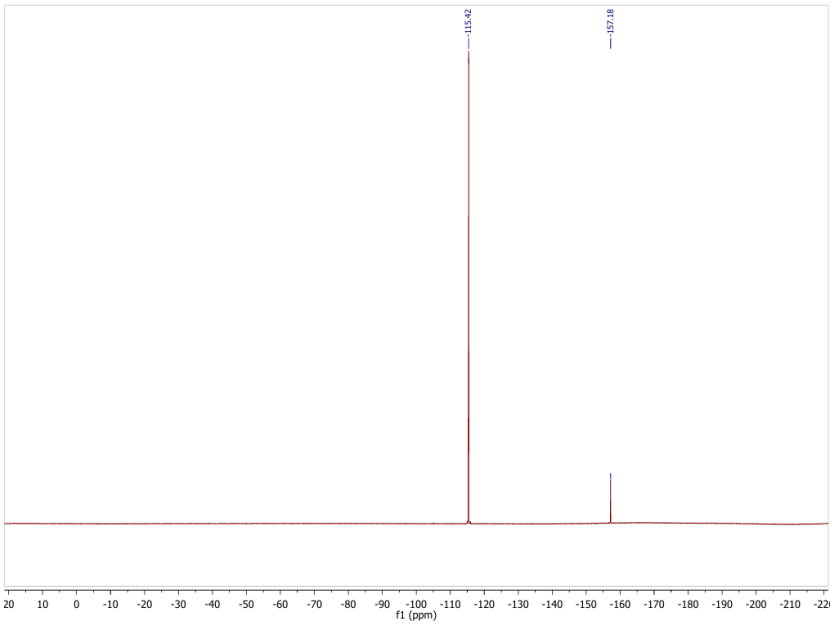

Figure 32: ^{19}F NMR of compound mixture **44**/**45** in CD_3OD with fluorobenzene as reference.

Upon complexation of the free ligand mixture **44**/**45** with zinc perchlorate to form complex mixture **46**/**47**, the major fluorotriazole peak moves downfield to -149.9 ppm, a change of 7.3 ppm (Figure 33b). This value is almost identical to that observed for compound **37** suggesting that the fluorine environment of **47** is extremely similar to complex **37**. Furthermore, the increase in the change of fluorine chemical shift (Δδ) from 6.5 ppm with **37** to 7.3 ppm for **46**/**47** suggests that complex mixture **46**/**47** may undergo a slightly larger structural rearrangement upon coordination. This is consistent with the presence of a longer carbon linker, which requires the triazole donor atom to be drawn further into the coordination sphere of the zinc centre as shown by Liu *et al*. who concluded that by increasing the linker length led to greater structural flexibility in metal complexes like these.[94] Kotková *et al.* previously synthesized tri-fluoro-methyl cyclam conjugates with differing pendant length,[60] and demonstrated that cyclam based Cu^{2+} complexes with progressively longer fluorinated pendant-linker spaces exhibit increasing ^{19}F relaxation times and narrower peak linewidths, confirming that longer pendant arms confer greater conformational flexibility. Upon addition of piperidine (100 equiv.), the major fluorine peak moves to -155.1 ppm with a minor satellite peak at -158.0 ppm, a comparable spectrum to that of the free ligand mixture **44**/**45** with added piperidine (Figure 33d).

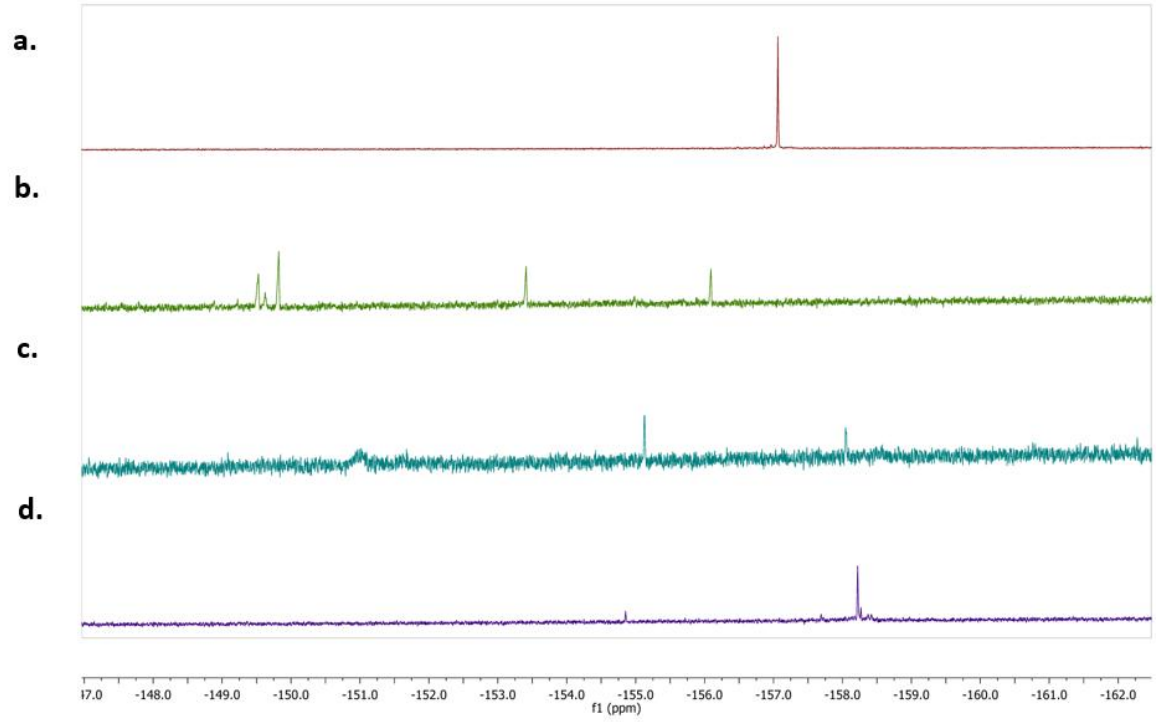

Figure 33: ^{19}F NMR visualization of triazole displacement with piperidine referenced to fluorobenzene. **a.** free ligand mixture **44**/**45**; **b.** zinc complex mixture **46**/**47**; **c. 46**/**47** + piperidine (100 equiv.); **d.** free ligand mixture **44**/**45** + piperidine (100 equiv.).

The ^{19}F NMR spectrum of the mixture of complexes **46**/**47** (Figure 33b) reveals multiple peaks in contrast to the free ligand mixture **44**/**45**. As discussed in Chapter 2, the presence of cyclam conformational isomers is expected which can be locked as configurational isomers upon metal complexation; however, the ^{19}F NMR signals for complex **37** (Figure 29b) are confined within a 1 ppm range, while those for complex mixture **46**/**47** span approximately 7 ppm. Additionally, the presence of five peaks suggests that as many as five different cyclam conformers may be present, an observation not previously reported in the literature. Alternatively, and more likely, there may be species present in this solution of **46**/**47** in which the triazole itself is not coordinated to the metal in contrast to complex **37**. This may be attributed to the longer carbon linker between cyclam and the triazole in **46**/**47**, which increases the distance between the triazole nitrogen donor and the zinc centre. This spatial separation can lead to weaker or absent coordination in some cases. Chernobryva *et al*. have reported that increasing the length of triazole linkers in tripodal ligands results in more distorted coordination geometries and reduced metal-binding stability.[95] Similarly, Keypour *et al*. investigated the effect of pendant arm length on metal coordination, observing that in a ligand with an ethylamino arm, the hydroxypropyl group coordinates to the Cu^{2+} centre, whereas in the longer propylamino analogue, the hydroxypropyl group remained uncoordinated (Figure 34).[96]

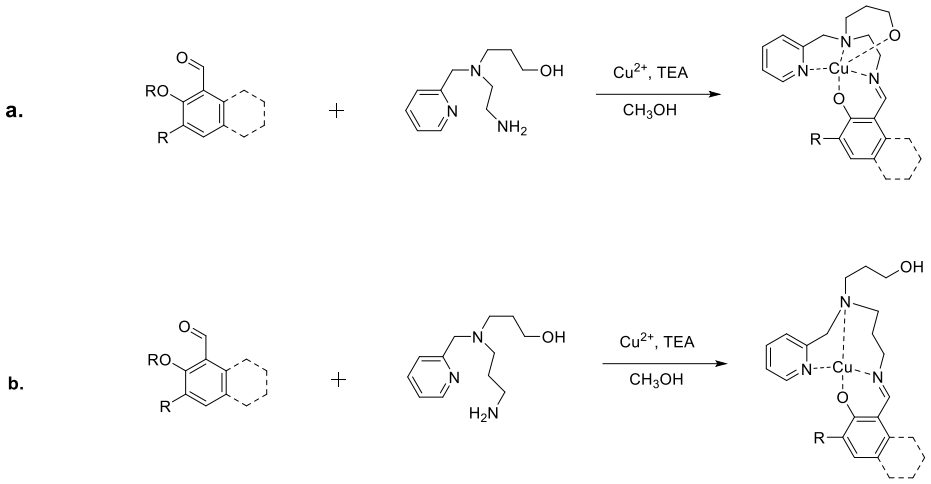

Figure 34. Copper complexes resulting from salicylaldehyde condensation with unsymmetrical triamines. **a.** Ethylamino-triamine with hydroxypropyl group coordinated to the Cu^{2+} centre. **b.** Propylamino-triamine with hydroxypropyl group un-coordinated to the Cu^{2+} centre.[96]

These hydroxypropyl moieties function similarly to triazole donor nitrogens as explored by Tabbì *et al*.,[97] especially in complexes with metals such as Zn^{2+} or Cu^{2+} suggesting that a comparable reduction in coordination may occur when triazole-containing arms are lengthened such as in complex mixture **46**/**47.**

As a result, the triazole of complex **46**/**47** has greater mobility and the fluorine occupies several different environments, which contributes to the wider range of chemical shifts observed in the ^{19}F NMR spectrum. Even with these additional peaks present, the observed shifts in the ^{19}F NMR spectrum upon addition of piperidine support the conclusion that triazole-zinc interactions are still occurring in this mixture, and that these interactions are at least partially displaced or disrupted by the coordinating amine.

3.3 Conclusions

This chapter details a series of ^{19}F NMR experiments carried out on zinc complexes **37** and **47** to visualise metal-triazole interactions and the displacement of the triazole from the metal using piperidine. The significant changes in chemical shift observed upon complexation with zinc and subsequent reversion upon addition of piperidine confirm that the triazole ring actively participates in coordination to the zinc centre and can be displaced by a suitable anion, and that this displacement can be clearly visualised using ^{19}F NMR spectroscopy. The use of fluorobenzene as a stable internal reference enabled accurate tracking of these changes. Even without being isolated in pure form, complex **47** still provides valuable insights into the effect of increasing the carbon chain linker on visualising triazole displacement. These findings

establish that 5-fluorotriazole-cyclam systems provide a reliable and highly responsive platform for monitoring coordination changes in metal complexes, supporting their potential in future sensing and biological applications in complex chemical environments, such as the monitoring of the hER-estradiol binding event.

3.4 Future work

3.4.1 Isolating C4 triazole connectivity complexes

By incorporating fluorinated triazoles, ^{19}F NMR studies can be employed to monitor coordination changes upon biological interactions, such as estradiol-hER and biotin-avidin binding events. While established routes have enabled the efficient synthesis of N1-substituted 5-fluorotriazoles, C4 connectivity has previously shown greater potential for detecting changes in metal coordination due to more pronounced spectrometric shifts. Simplifying the synthesis of C4-substituted 5-fluorotriazoles would improve the utility of these systems in probing coordination geometry.

3.4.2 Functionalising estrogens for ^{19}F NMR sensing of estrogen-hER binding interactions

Having demonstrated the ^{19}F NMR approach for monitoring metal-triazole coordination in Chapter 3. The next step is to apply this approach to monitor a 'real world' biological interaction. A specific target of interest is the estrogen-hER interaction which has previously been explored in the Rutledge group.[98] To study whether the ^{19}F NMR approach can be utilised to monitor estrogen-hER binding, suitably functionalised estrogen derivatives that can be coupled (CuAAC) to obtain the target cyclam-5-fluorotriazole-estradiol system are required.

Three common estrogen derivatives: estrone, ethinylestradiol and 17-beta estradiol each provide unique ways to functionalise a suitable CuAAC partner. Preliminary experiments to protect the highly reactive phenol group in each derivative with mesylates or benzyl groups have been successful. Protection of the phenol group is important as the electron-donating effect of the hydroxyl group makes targeting solely the 17th position of the estrogen derivatives difficult. These next steps could allow for the synthesis of estradiols into useful compounds for the ^{19}F NMR experiments.

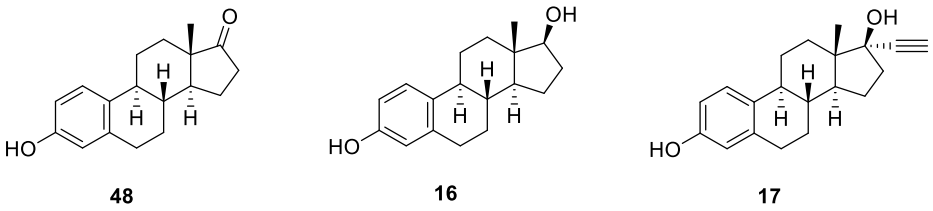

Figure 35. Structures of common estrogen derivatives: estrone **48**, ethinylestradiol **16**, and 17-beta estradiol **17**.

Proposed functionalisation routes to a suitable CuAAC click partner:

One approach involves functionalising estrone **48** at C17 by introducing a terminal alkyne, which can then be iodinated following the procedures outlined in Chapter 2 (Scheme 2.3); previous work in the Rutledge group has already demonstrated that estrone can undergo propargyl Grignard addition at this position..[98]

Ethinylestradiol **16** presents a second route, as its native terminal alkyne can also be iodinated to give a suitable 1-iodoalkyne derivative, although it remains uncertain whether the short tether provides sufficient flexibility to avoid steric hindrance during the CuAAC reaction, an issue highlighted by Zhu et al., who showed that steric bulk near the metal centre can restrict azide or alkyne access.[99]

A third strategy involves 17-beta estradiol **17**, where nucleophilic substitution at the 17-OH position could be used to introduce a longer, more flexible spacer incorporating either an azide or a terminal alkyne (which could then be iodinated), thereby reducing steric congestion during CuAAC coupling.

By obtaining either a 1-iodoalkyne or an azide as a CuAAC partner, previous reported steps in Chapter 2 (Scheme 2.3) can by utilized to obtain potentially useful probes for utilising ^{19}F NMR experiments to monitor the ‘real world’ estrogen-hER interaction.

Chapter 4 – Experimental

4.1 General Materials and Instrumentation

Acetonitrile, dichloromethane, diethyl ether, dimethylformide, methanol and tetrahydrofuran were collected fresh from a PureSolv MD 7 solvent purification system having been passed through anhydrous alumina columns. For experiments not requiring anhydrous conditions, HPLC grace acetonitrile and methanol were used without further purification. All commercially available reagents and solvents were purchased from Sigma Aldrich, Alfa Aesar, Matrix Scientific, Merck Millipore or Ajax Finechem and used without purification. Flash column chromatography was performed on Chem-Supply 0.04 – 0.06 mm (230 – 400 mesh) silica gel. Automated flash column chromatography was performed on a Biotage Isolera Spektra One using Biotage Snap KP-Sil cartridges and their default flow rates. TLC analyses were performed on Merck silica gel 60 F_{254} pre-coated aluminium plates (0.2 mm) and visualised with UV (254 and 365 nm), followed by staining with potassium permanganate or vanillin.

^{1}H, ^{13}C, ^{19}F nuclear magnetic resonance (NMR) spectra were recorded on a Bruker Advance 300 or 500 spectrometer. Chemical shifts are reported in δ ppm relative to trimethylsilane (δ = 0) or residual solvent resonance as an internal standard. Mass spectra (LRMS) were acquired on Bruker amazon SL mass spectrometer. Accurate mass measurements (HRMS) were performed on a Bruker Apex Qe 7T Fourier Transform Ion Cyclotron Resonance (FT-ICR) mass spectrometer. Matrix Assisted Laser Desorption Ionisation Time of Flight (MALDI-TOF) mass spectra were acquired on a Bruker autoFlex Speed LRF in a positive reflectron mode.

Infrared spectra were recorded on a Bruker ALPHA FT-IR spectrophotometer (ZnSe or diamond ATR). LCMS analysis was carried out on a Shimadzu LCMS-2020 system using a Water Sunfire™ C18 column (5 μm, 2.1 x 150 mm) at a flow rate of 0.2 mL/min with a gradient of 0 – 100% B over 20 minutes; mobile phases of 0.1% formic acid in Milli-Q water (Solvent A) and 0.1% formic acid in acetonitrile (solvent B) were used.

4. 2 Synthetic Procedures

Safety note: *Sodium azide, organic azides and perchlorate salts of metal complexes with organic ligands are potentially explosive. Only small amounts of material should be prepared, and these should be handled with caution.*

4.2.1 General Procedures

General Synthetic Procedure A: *Iodination of primary alkynols.*

Alkynol (1 equiv.) was dissolved in MeOH (10 mL). A solution of NaOH (3.99 g, 1.0 mol) in H_2O (10 mL) was prepared, cooled to 0°C and added to the reaction mixture. I_2 (0.88 equiv.) was added in one portion and the solution was stirred at room temperature overnight. The organic phase was neutralised with 1M HCl and extracted with Et_2O. The organic phase was washed with saturated $Na_2S_2O_3$, dried over $MgSO_4$ and concentrated under reduced pressure to afford the desired iodinated primary alkynol.

General Synthetic Procedure B: *The Copper(I)-Catalyzed Azide Alkyne Cycloaddition (CuAAC).*

For 0.05 – 1.0 mmol scale.

Iodo-alkyne (1 equiv.) and azide (1.2 equiv.) were dissolved in THF (10 mL) and added to CuI (0.05 equiv.) in THF (2 mL). TEA (2 equiv.) was added, and the mixture was stirred under N_2 for 6 h. The mixture was quenched with saturated NH_4Cl (10 mL). The THF was removed under reduced pressure and the remaining mixture was extracted with EtOAc (2 x 20 mL). The combined organic extracts were dried ($MgSO_4$) and concentrated under reduced pressure. The residue was purified by flash column chromatography to afford the desired click product.

General Synthetic Procedure C: *Conversion of 5-iodotriazoles to 5-fluorotriazoles.*

5-Iodotriazole (1 equiv.) was dissolved in MeCN (2 mL) and added to a 2-5 mL round-bottomed microwave vial. Potassium fluoride (5 equiv.) was added to the mixture and the solids were washed off the side with H_2O (2 mL). The mixture was stirred for several minutes before being capped with the appropriate Teflon microwave lid. The vial was placed into the microwave reactor set to “Very High” adsorption and heated at 160 °C for 15 min. The mixture was extracted with EtOAc (3 x 5 mL), dried ($MgSO_4$) and concentrated under reduced pressure. The residue was purified by flash column chromatography to afford the desired 5-fluorotriazole.

General Synthetic Procedure D: *Alkylation of tri-Boc-cyclam with 5-fluorotriazoles.*

To a solution of 5-fluorotriazole (2 equiv.) in DCM (5 mL) were added TEA (3 equiv.) and methanesulfonyl chloride (3 equiv.). The reaction mixture was stirred at room temperature for 16 h. Saturated aqueous $NaHCO_3$ was added, and the organic layer was washed with brine (5 mL), dried ($MgSO_4$) and concentrated under reduced pressure. The residue was dissolved in MeCN (5 mL) and added to a solution of tri-Boc-cyclam (1 equiv.) in MeCN (5 mL). Sodium iodide (1 equiv.) and potassium carbonate (5 equiv.) were added, and the mixture was stirred under reflux for 16 h. The

solution was cooled, extracted with EtOAc (3 x 20 mL), dried ($MgSO_4$) and concentrated under reduced pressure. The residue was purified by flash column chromatography to afford the desired alkylated tri-Boc-cyclam.

General Synthetic Procedure E: *HCl-Mediated Boc deprotection and basification of HCl salt.*
To a solution of Boc-protected cyclam in dioxane (3 mL) was added a solution of HCl (4M in dioxane, 3 mL). The reaction mixture was stirred at room temperature for 16 h. The residue was concentrated under reduced pressure. The residue was dissolved in MeOH (10 mL) and a suspension of excess Ambersep® 900 resin (hydroxide form, pre-swelled with H_2O for 15 min and MeOH for 15 min) in MeOH (5 mL) was added. The mixture was stirred at room temperature for 15 min, filtered and concentrated under reduced pressure to afford the desired deprotected cyclam.

General Synthetic Procedure F: *Zinc complexation from free base.*
For < 0.15 mmol scale.
To a solution of free base cyclam ligand (1 equiv.) in EtOH (3 mL) was added a solution of $Zn(ClO_4)_2 \cdot 6H_2O$ (1.1 equiv.) in EtOH (2 mL). The reaction mixture was stirred at room temperature for 16 h, filtered and concentrated under reduced pressure to afford the desired metal complex.

4.2.2 Compounds first described in Chapter Two

*Benzyl azide **21***

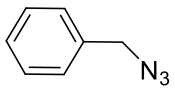

To a solution of benzyl bromide (0.5 mL, 4.2 mmol) in acetone (3 mL) and water (3 mL) was added sodium azide (0.95 g, 15.1 mmol). The reaction was stirred at room temperature for 2 h. The reaction was diluted with water (5 mL), extracted with diethyl ether (3 x 5 mL) and dried ($MgSO_4$). The organic layer was concentrated under rotary evaporation to yield the desired product **21** as a clear oil (0.54 g, 4.1 mmol, 97%). **^{1}H NMR** (300 MHz, $CDCl_3$): δ 4.32 (s, 2H), 7.28-7.42 (m, 5H); **^{13}C NMR** (75 MHz, $CDCl_3$): 54.42, 127.42, 128.01, 128.69, 128.98, 132.64. The spectroscopic data were in agreement with those in literature.[100]

*Tri-tert-butyl 1,4,8,11-tetraazacyclotetradecane-1,4,8-tricarboxylate **26***

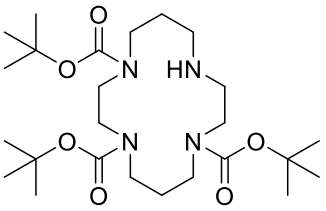

To a solution of cyclam (1.66 g, 8.29 mmol) and triethylamine (5.70 mL, 41 mmol) in anhydrous DCM (400 mL) was added dropwise di-tert-butyl dicarbonate (3.24 g, 14.8 mmol) in anhydrous DCM (90 mL) under an atmosphere of N_2. After the addition was complete, the reaction mixture was cooled to -15°C. A second portion of di-tert-butyl dicarbonate (2.15 g, 9.87 mmol) in anhydrous DCM (90 mL) was added dropwise. The solution was stirred at room temperature overnight and washed with saturated $NaHCO_3$ (2x200 mL) and brine (200 mL). The organic phase was dried ($MgSO_4$) and concentrated under reduced pressure. The residue was purified by flash column chromatography (EtOAc) to afford tri-Boc-cyclam **26** as a pale-yellow oil (2.94 g, 70%). **^{1}H NMR** (300 MHz, $CDCl_3$): δ 1.46 (s, 27H), 1.64-1.77 (m, 2H), 1.84-2.01 (m, 2H), 2.62 (t, 2H), 2.79 (t, 2H), 3.17-3.53 (m, 12H); **LRMS** (ESI+): *m/z* 501.34 ($[M+H]^+$, 100%), 523.32 ($[M+Na]^+$, 87%). The spectroscopic data were in agreement with those in literature.[101]

*2-Azidoethyl 4-methylbenzenesulfonate **27***

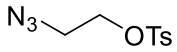

To a solution of bromoethanol (1.60 g, 12.8 mmol) in water (10 mL) was added sodium azide (1.11 g, 17.1 mmol). The mixture was stirred at reflux for 16 h. The solution was cooled before being extracted with ethyl acetate (2 x 15 mL). The combined organic layers were washed with brine (25 mL) and dried ($MgSO_4$). To the organic solution was added triethylamine (5 mL, 36 mmol) and toluenesulfonyl chloride (3.53 g, 18.5 mmol) and the mixture was stirred at room temperature for 16h. The solution was washed with NaOH (2.5M, 25 mL), brine (25 mL), dried ($MgSO_4$) and concentrated under reduced pressure. The residue was purified by flash column chromatography (EtOAc: Pet Benz = 3:7) to afford the desired azide **27** as a clear oil (1.92 g, 62%). **^{1}H NMR** (300 MHz, $CDCl_3$): δ 2.46 (s, 3H), 3.49 (t, 2H), 4.16 (t, 2H), 7.37 (m, 2H), 7.82 (m, 2H); **^{13}C NMR** (75 MHz, $CDCl_3$): 21.78, 49.66, 68.12, 127.97, 130.04, 132.68, 145.28. The spectroscopic data were in agreement with those in literature.[102]

Tri-tert-butyl 11-(2-azidoethyl)-1,4,8,11-tetraazacyclotetradecane-1,4,8-tricarboxylate ***28***

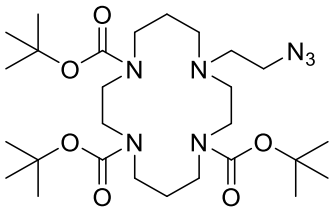

To a solution of tri-Boc-cyclam (60 mg, 0.12 mmol) in MeCN (5 mL) were added azidoethyl toluenesulfonate (73 mg, 0.61 mmol), potassium carbonate (250 mg, 4.72 mmol) and sodium iodide (91 mg, 0.61 mmol). The reaction mixture was stirred at reflux for 48 h. Water (10 mL) was added, and the product was extracted with ethyl acetate (2 x 10 mL). The extracts were combined and concentrated under pressure using rotary evaporation. The residue was purified by flash column chromatography (EtOAc:Pet Benz = 1:19 ramping to EtOAc:Pet Benz = 3:7) to yield the desired product **28** as a yellow oil (60 mg, 88%). **^{1}H NMR** (300 MHz, $CDCl_3$): δ 1.46 (s, 27H), 1.69 (m, 2H), 1.88 (m, 2H), 2.46 (m, 2H), 2.62 (m, 4H), 3.14-3.52 (m, 14H); **LRMS** (ESI+): *m/z* 570.52 ($[M+H]^+$, 100%), 592.38 ($[M+Na]^+$, 36%). The spectroscopic data were in agreement with those in literature.[45]

1-Iodo-phenylacetylene ***22***

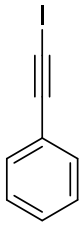

Phenylacetylene (100 mg, 0.98 mmol) was dissolved in THF (5 mL) and treated with CuI (16.2 mg, 0.09 mmol) and N-iodomorpholine hydroiodide (369 mg, 1.01 mmol). The reaction mixture was stirred at room temperature for 16 h. The suspension was poured onto a pad of activated neutral alumina (50 mL), and the filtrate was collected under vacuum. The solid phase was washed with DCM (4 x 5 mL) and the combined organic fractions were concentrated under reduced pressure using rotary evaporation to give 1-iodo-phenylacetylene **22** as an orange oil (208 mg, 93%). **^{1}H NMR** (300 MHz, $CDCl_3$): δ 7.28-7.34 (m, 3H), 7.39-7.47 (m, 2H); **^{13}C NMR** (75 MHz, $CDCl_3$): 6.03, 94.16, 123.47, 128.16, 128.83, 132.41. The spectroscopic data were in agreement with those in literature.[103]

*Tri-tert-butyl 11-(2-(5-iodo-4-phenyl-1H-1,2,3-triazol-1-yl)ethyl)-1,4,8,11-tetraazacyclotetradecane-1,4,8-tricarboxylate **29***

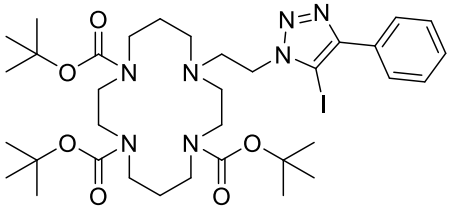

Tri-Boc-azidoethylcyclam **28** (50 mg, 0.09 mmol) and 1-iodo-phenylacetylene **22** (41 mg, 0.18 mmol) were reacted using General Synthetic Procedure B. The crude product was purified by flash column chromatography (EtOAc:Pet Benz = 3:7 ramping to 8:2) to yield the desired product **29** as a yellow solid (33 mg, 46%). **^{1}H NMR** (300 MHz, $CDCl_3$): δ 1.46 (s, 27H), 1.58-1.87 (m, 8H), 2.58 (m, 2H), 2.74 (m, 2H), 3.00 (t, 2H), 3.15-3.45 (m, 12H), 4.50 (t, 2H), 7,44 (m, 3H), 7.92 (d, 2H); **^{13}C NMR** (75 MHz, $CDCl_3$): 28.42, 45.55, 48.24, 54.50, 79.85, 127.50, 128.62, 130.18, 149.87, 155.51; **LRMS** (ESI+): *m/z* 798.31 ($[M+H]^+$, 16%), 820.31 ($[M+Na]^+$, 100%); **HRMS** (ESI+): m/z Calcd. for $C_{35}H_{56}IN_7NaO_6^+$ $[M+Na^+]$ 820.32290; found 820.32233; **FTIR** (ATR) ν_{max}/cm^{-1}: 2973, 2934, 1683, 1463, 1409, 1364, 1234, 1154, 770, 735.

3-Iodoprop-2-yn-1-ol ***32***

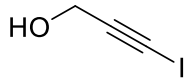

2-Propyn-1-ol (1.00g, 5.50 mmol) was reacted using General Synthetic Procedure A and the product was purified by flash column chromatography (EtOAc: Pet Benz = 1:9 ramping to 3:7) to yield the desired **32** product as an orange oil (1.67 g, 48%). **^{1}H NMR** (300 MHz, $CDCl_3$): δ 4.42 (s, 2H); **^{13}C NMR** (75 MHz, $CDCl_3$): 2.75, 52.71, 92.60. The spectroscopic data were in agreement with those in literature.[104]

(1-Benzyl-5-iodo-1H-1,2,3-triazol-4-yl)methanol ***33***

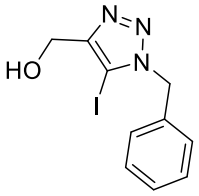

Benzyl azide **21** (0.52 g, 3.90 mmol) and 3-iodoprop-2-yn-1-ol **32** (0.52 g, 2.84 mmol) were reacted using General Synthetic Procedure B and the product was purified by flash column chromatography (EtOAc: Pet Benz = 2:8 ramping to 4:6) to yield the desired product **33** as a yellow solid (0.41g, 49%). **^{1}H NMR** (300 MHz, $CDCl_3$): δ 2.36 (t, 1H), 4.72 (d, 2H), 5.59 (s, 2H), 7.27-7.42 (m, 5H); **^{13}C NMR** (75 MHz, $CDCl_3$): 54.26, 56.72, 127.87, 128.60, 129.05, 134.12, 151.19; **LRMS** (ESI+): *m/z* 337.87 ($[M+Na]^+$, 45%), 652.81 ($[2M+Na]^+$, 100%); **HRMS** (ESI+): m/z Calcd. for $C_{10}H_{10}IN_3NaO^+$ $[M+Na^+]$ 337.97608; found 337.97609; **FTIR** (ATR) ν_{max}/cm^{-1}: 3151, 1494, 1452, 1365, 1269, 1223, 1143, 1084, 1008, 800.

(1-Benzyl-5-fluoro-1H-1,2,3-triazol-4-yl)methanol ***34***

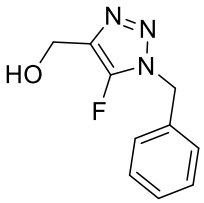

(1-Benzyl-5-iodo-1H-1,2,3-triazol-4-yl)methanol **33** (0.45 g, 1.43 mmol) was reacted using General Synthetic Procedure C and the product was purified by flash column chromatography (EtOAc: Pet Benz = 1:9 ramping to 8:2) to yield the desired product **34** as an orange oil (0.20 g, 69%). **^{1}H NMR** (300 MHz, $CDCl_3$): δ 2.29 (t, 1H), 4.70 (d, 2H), 5.41 (s, 2H,), 7.29-7.43 (m, 5H); **^{19}F NMR** (300 MHz,

$CDCl_3$): -153.83; **^{13}C NMR** (75 MHz, $CDCl_3$): 51.14, 54.27, 128.01, 128.84, 129.13, 133.38, 148.37; **LRMS** (ESI+): *m/z* 230.11 ([M+Na]$^+$, 66%), 437.11 ([2M+Na]$^+$, 100%); **HRMS** (ESI+): m/z Calcd. for $C_{10}H_{10}FN_3NaO^+$ [M+Na$^+$] 230.07001; found 230.06981; **FTIR** (ATR) ν_{max}/cm^{-1}: 3307, 1619, 1515, 1454, 1284, 1222, 1018, 732.

*Tri-tert-butyl 11-((1-benzyl-5-fluoro-1H-1,2,3-triazol-4-yl)methyl)-1,4,8,11-tetraazacyclotetradecane-1,4,8-tricarboxylate **35***

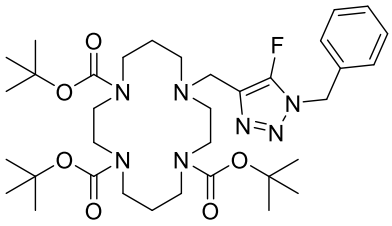

(1-Benzyl-5-fluoro-1H-1,2,3-triazol-4-yl)methanol **34** (93.8 mg, 0.45 mmol) was reacted using General Synthetic Procedure D and the resulting product was purified by flash column chromatography (EtOAc: Pet Benz = 5:5 ramping to 8:2) to yield the desired product **35** as a yellow solid (223 mg, 72%). **^{1}H NMR** (300 MHz, $CDCl_3$): δ 1.46 (m, 27H), 1.69 (m, 2H), 1.85 (m, 2H), 2.41 (m, 2H), 2.62 (m, 2H), 3.15-3.46 (m, 12H), 3.71 (s, 2H), 5.40 (s, 2H), 7.28-7.42 (m, 5H); **^{19}F NMR** (300 MHz, $CDCl_3$): -153.98; **^{13}C NMR** (75 MHz, $CDCl_3$): 28.55, 29.59, 45.25, 46.30, 48.59, 51.12, 79.51, 127.84, 128.78, 129.23, 133.60, 155.58; **LRMS** (ESI+): *m/z* 690.12 ([M+H]$^+$,66%), 712.41 ([M+Na]$^+$,100%); **HRMS** (ESI+): m/z Calcd. for $C_{35}H_{56}FN_7NaO_6^+$ [M+Na$^+$] 712.41683; found 712.41673; **FTIR** (ATR) ν_{max}/cm^{-1}: 2970, 2929, 1700, 1490, 1401, 1350, 1150, 900, 790, 750.

*1-((1-Benzyl-5-fluoro-1H-1,2,3-triazol-4-yl)methyl)-1,4,8,11-tetraazacyclotetradecane **36***

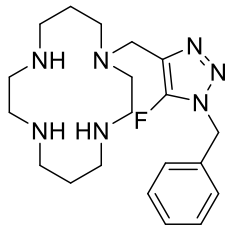

Tri-tert-butyl 11-((1-benzyl-5-fluoro-1H-1,2,3-triazol-4-yl)methyl)-1,4,8,11-tetraazacyclotetradecane-1,4,8-tricarboxylate **35** (240 mg, 0.35 mmol) was deprotected using General Synthetic Procedure E to yield the desired product as a sticky orange solid (134 mg, 98%) **^{1}H NMR** (300 MHz, MeOD): δ 1.65 (m, 2H), 1.87 (m, 2H), 2.42-2.80 (m, 16H) 3.73 (s, 2H), 5.52 (s, 2H), 7.21-7.47 (m, 5H); **^{19}F NMR** (300

MHz, $CDCl_3$): -154.29; **^{13}C NMR** (75 MHz, $CDCl_3$): 26.28, 29.05, 45.58 47.60, 50.72, 51.53, 52.08, 54.40, 55.06, 124.86, 129.09, 129.85, 130.15, 135.60; **LRMS** (ESI+): m/z 390.25 ($[M+H]^+$, 100%); **HRMS** (ESI+): m/z Calcd. for $C_{20}H_{34}FN_7^+$ $[M+H^+]$ 390.27760; found 390.27763; **FTIR** (ATR) v_{max}/cm^{-1}: 2950, 2817, 1608, 1455, 1284, 1114, 729, 698.

*Zinc perchlorate complex of 1-((1-benzyl-5-fluoro-1H-1,2,3-triazol-4-yl)methyl)-1,4,8,11-tetraazacyclotetradecane **37***

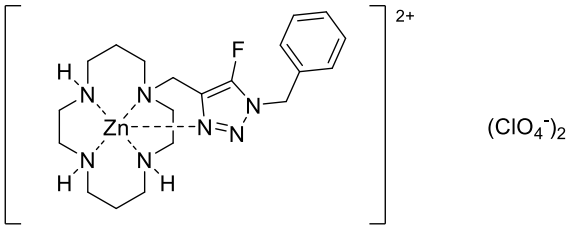

1-((1-Benzyl-5-fluoro-1H-1,2,3-triazol-4-yl)methyl)-1,4,8,11-tetraazacyclotetradecane **36** (120 mg, 0.31 mmol) was complexed using General Synthetic Procedure F to yield the desired product **37** as a brown solid (92 mg, 46%). **LRMS** (ESI+): *m/z* 553.11 ($[M+H-ClO_4]^+$,100%) **HRMS** (ESI+): m/z Calcd. for $C_{20}H_{32}ClFN_7O_4Zn^+$ $[M-ClO_4]^+$ 552.14743; found 552.14827; **FTIR** (ATR) v_{max}/cm^{-1}: 3230, 2913, 1601, 1456, 1063, 987, 740, 620.

*4-Iodobut-3-yn-1-ol **39***

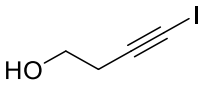

3-Butyn-1-ol (1.48 g, 21.1 mmol) was reacted using General Synthetic Procedure A and the product was purified by flash column chromatography (EtOAc:Pet Benz = 2:8 ramping to 4:6) to yield the desired product **39** as a yellow solid (2.33 g, 56%). **^{1}H NMR** (300 MHz, $CDCl_3$): δ 2.24 (s, 1H), 2.63 (t, 2H), 3.73 (m, 2H); **^{13}C NMR** (75 MHz, $CDCl_3$): -4.33, 25.12, 61.06, 91.33. The spectroscopic data were in agreement with those in literature.[105]

*2-(5-Iodo-4-phenyl-1H-1,2,3-triazol-1-yl)ethan-1-ol **40***

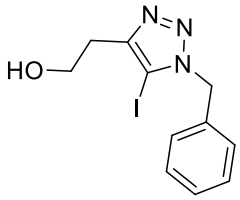

Benzyl azide **21** (1.36 g, 10.2 mmol) and 4-iodobut-3-yn-1-ol **39** (2.00 g, 10.2 mmol) were reacted using General Synthetic Procedure B and the product was purified by flash column chromatography (EtOAc: Pet Benz = 1:9 ramping to 4:6) to yield the desired product **40** as a white solid (1.57 g, 47%). **^{1}H NMR** (300 MHz, $CDCl_3$): δ 2.88 (t, 2H), 4.00 (m, 2H), 5.59 (s, 2H), 7.27-7.42 (m, 5H); **^{13}C NMR** (75 MHz, $CDCl_3$): 29.14, 54.40, 61.15, 127.85, 128.64, 128.96, 134.25, 150.33; **LRMS** (ESI+): *m/z* 351.97 ($[M+Na]^+$, 100%), 680.84 ($[2M+Na]^+$, 17%); **HRMS** (ESI+): m/z Calcd. for $C_{11}H_{12}IN_3NaO^+$ $[M+Na^+]$ 351.99173; found 351.99201; **FTIR** (ATR) ν_{max}/cm^{-1}: 3298, 1620, 1494, 1431, 1289, 1212, 1042, 722, 697.

*2-(5-Fluoro-4-phenyl-1H-1,2,3-triazol-1-yl)ethan-1-ol **41***

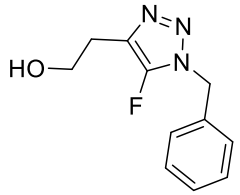

2-(5-iodo-4-phenyl-1H-1,2,3-triazol-1-yl)ethan-1-ol **40** (0.25 g, 0.74 mmol) was reacted using General Synthetic Procedure C and the product was purified by flash column chromatography (EtOAc: Pet Benz = 1:9 ramping to 8:2) to yield the desired product **41** as an orange oil (0.11 g, 73 %). **^{1}H NMR** (300 MHz, $CDCl_3$): δ 2.84 (t, 2H), 3.95 (t, 2H), 5.39 (s, 2H), 7.28-7.42 (m, 5H); **^{19}F NMR** (300 MHz, $CDCl_3$): -156.27; **^{13}C NMR** (75 MHz, $CDCl_3$): (75 MHz, $CDCl_3$): 26.68, 51.14, 60.91, 128.01, 128.87, 129.09, 133.55, 145.54; **LRMS** (ESI+): *m/z* 222.13 ($[M+H]^+$, 100%) **HRMS** (ESI+): m/z Calcd. for $C_{22}H_{24}F_2N_6NaO_2^+$ $[2M+Na^+]$ 465.18210; found 465.18239. **FTIR** (ATR) ν_{max}/cm^{-1}: 3338, 1620, 1496, 1454, 1048, 729, 697.

*Tri-tert-butyl 11-(2-(1-benzyl-5-(fluoro/iodo)-1H-1,2,3-triazol-4-yl)ethyl)-1,4,8,11-tetraazacyclotetradecane-1,4,8-tricarboxylate **42/43***

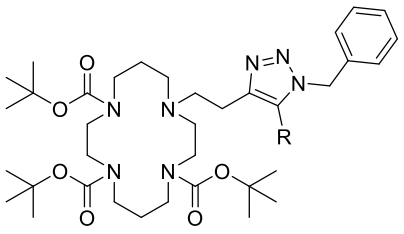

42, R = I
43, R = F

2-(5-Fluoro-4-phenyl-1H-1,2,3-triazol-1-yl)ethan-1-ol **41** (0.10 g, 0.45 mmol) was reacted using General Synthetic Procedure D and the resulting product was purified by flash column chromatography (EtOAc: Pet Benz = 5:5 ramping to 8:2) to yield a (1:2) mixture of **42/43** as a yellow solid (161 mg). **LRMS** (ESI+): *m/z* 704.44 ([M(**43**)+H]$^+$, 100%), 726.43 ([M(**43**)+Na]$^+$, 68%), 812.33 ([M(**42**)+H]$^+$, 31%), 834.27 ([M(**42**)+Na]$^+$, 20%) **HRMS** (ESI+): m/z Calcd. for $C_{36}H_{58}FN_7O_6^+$ [M(**43**)+H$^+$] 704.45054; found 704.44973.

*1-(2-(1-Benzyl-5-(fluoro/iodo)-1H-1,2,3-triazol-4-yl)ethyl)-1,4,8,11-tetraazacyclotetradecane **44/45***

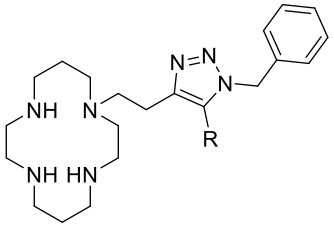

44, R = I
45, R = F

Tri-tert-butyl 11-(2-(1-benzyl-5-(fluoro/iodo)-1H-1,2,3-triazol-4-yl)ethyl)-1,4,8,11-tetraazacyclotetradecane-1,4,8-tricarboxylate **42/43** (150 mg) was deprotected using General Synthetic Procedure E to yield a (3:7) mixture of **44/45** as a sticky yellow solid (78 mg). **LRMS** (ESI+): *m/z* 404.26 ([M(**45**)+H]$^+$, 100%), 511.21 ([M(**44**)+H]$^+$, 30%) **HRMS** (ESI+): m/z Calcd. for $C_{21}H_{35}FN_7^+$ [M(**45**)+H$^+$] 404.29325; found 404.29293.

*Zinc perchlorate complex of 1-(2-(1-benzyl-5-(fluoro/iodo)-1H-1,2,3-triazol-4-yl)ethyl)-1,4,8,11-tetraazacyclotetradecane **46/47***

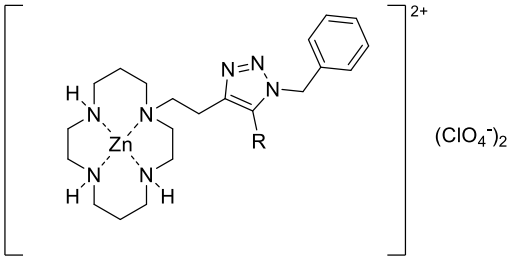

46, R = I
47, R = F

1-(2-(1-Benzyl-5-(fluoro/iodo)-1H-1,2,3-triazol-4-yl)ethyl)-1,4,8,11-tetraazacyclotetradecane **44/45** was complexed using General Synthetic Procedure F to yield a mixture of **46**/**47** as a brown solid (64 mg). **LRMS** (ESI+): *m/z* 566.15 ([M(**47**)+H]$^+$, 100%), 674.03 ([M(**46**)+H]$^+$, 33%) **HRMS** (ESI+): m/z Calcd. for $C_{21}H_{34}ClFN_7O_4Zn^+$ [M(**47**)-ClO_4]$^+$ 566.16308; found 566.16398.

References

(1) Uddin, T. M.; Chakraborty, A. J.; Khusro, A.; Zidan, B. M. R. M.; Mitra, S.; Emran, T. B.; Dhama, K.; Ripon, M. K. H.; Gajdács, M.; Sahibzada, M. U. K.; et al. Antibiotic resistance in microbes: History, mechanisms, therapeutic strategies and future prospects. *Journal of Infection and Public Health* **2021**, *14* (12), 1750-1766. DOI: https://doi.org/10.1016/j.jiph.2021.10.020.

(2) Mcquitty, R. J. Metal-based drugs. *Science Progress* **2014**, *97* (1), 1-19.

(3) Boros, E.; Dyson, P. J.; Gasser, G. Classification of metal-based drugs according to their mechanisms of action. *Chem* **2020**, *6* (1), 41-60.
(4) Anthony, E. J.; Bolitho, E. M.; Bridgewater, H. E.; Carter, O. W.; Donnelly, J. M.; Imberti, C.; Lant, E. C.; Lermyte, F.; Needham, R. J.; Palau, M. Metallodrugs are unique: Opportunities and challenges of discovery and development. *Chemical Science* **2020**, *11* (48), 12888-12917.
(5) Ghosh, S. Cisplatin: The first metal based anticancer drug. *Bioorganic chemistry* **2019**, *88*, 102925.
(6) Frei, A.; Zuegg, J.; Elliott, A. G.; Baker, M.; Braese, S.; Brown, C.; Chen, F.; G. Dowson, C.; Dujardin, G.; Jung, N.; et al. Metal complexes as a promising source for new antibiotics. *Chemical Science* **2020**, *11* (10), 2627-2639, 10.1039/C9SC06460E. DOI: 10.1039/C9SC06460E.
(7) Dutescu, I. A.; Hillier, S. A. Encouraging the Development of New Antibiotics: Are Financial Incentives the Right Way Forward? A Systematic Review and Case Study. *Infect Drug Resist* **2021**, *14*, 415-434. DOI: 10.2147/idr.S287792 From NLM.
(8) Crișan, G.; Moldovean-Cioroianu, N. S.; Timaru, D. G.; Andrieș, G.; Căinap, C.; Chiș, V. Radiopharmaceuticals for PET and SPECT Imaging: A Literature Review over the Last Decade. *Int J Mol Sci* **2022**, *23* (9). DOI: 10.3390/ijms23095023 From NLM.
(9) Lohrke, J.; Frenzel, T.; Endrikat, J.; Alves, F. C.; Grist, T. M.; Law, M.; Lee, J. M.; Leiner, T.; Li, K. C.; Nikolaou, K.; et al. 25 Years of Contrast-Enhanced MRI: Developments, Current Challenges and Future Perspectives. *Adv Ther* **2016**, *33* (1), 1-28. DOI: 10.1007/s12325-015-0275-4 From NLM.
(10) Ceballos-Ceballos, J.; Loza-Gallardo, D. A.; Barajas-Romero, M. A.; Cantú-Brito, C.; Valdés-Ferrer, S. I. Recognition of Brain Metastases Using Gadolinium-Enhanced SWI MRI: Proof-of-Concept Study. *Frontiers in Neurology* **2020**, *Volume 11 - 2020*, Brief Research Report. DOI: 10.3389/fneur.2020.00005.
(11) Panagiotidis, E.; Alshammari, A.; Michopoulou, S.; Skoura, E.; Naik, K.; Maragkoudakis, E.; Mohmaduvesh, M.; Al-Harbi, M.; Belda, M.; Caplin, M. E.; et al. Comparison of the Impact of ⁶⁸Ga-DOTATATE and ¹⁸F-FDG PET/CT on Clinical Management in Patients with Neuroendocrine Tumors. *Journal of Nuclear Medicine* **2017**, *58* (1), 91-96. DOI: 10.2967/jnumed.116.178095.
(12) Iyad, N.; Ahmad, M. S.; Alkhatib, S. G.; Hjouj, M. Gadolinium contrast agents-challenges and opportunities of a multidisciplinary approach: Literature review. *European Journal of Radiology Open* **2023**, *11*, 100503.
(13) Reiter, T.; Ritter, O.; Prince, M. R.; Nordbeck, P.; Wanner, C.; Nagel, E.; Bauer, W. R. Minimizing Risk of Nephrogenic systemic fibrosis in Cardiovascular Magnetic Resonance. *Journal of Cardiovascular Magnetic Resonance* **2012**, *14* (1), 29. DOI: https://doi.org/10.1186/1532-429X-14-31.
(14) Dasari, S.; Tchounwou, P. B. Cisplatin in cancer therapy: molecular mechanisms of action. *European journal of pharmacology* **2014**, *740*, 364-378.

(15) Ott, I. 3.32 - Biodistribution of Metals and Metallodrugs. In *Comprehensive Inorganic Chemistry II (Second Edition)*, Reedijk, J., Poeppelmeier, K. Eds.; Elsevier, 2013; pp 933-949.
(16) Elmorsy, E. A.; Saber, S.; Hamad, R. S.; Abdel-Reheim, M. A.; El-kott, A. F.; AlShehri, M. A.; Morsy, K.; Salama, S. A.; Youssef, M. E. Advances in understanding cisplatin-induced toxicity: Molecular mechanisms and protective strategies. *European Journal of Pharmaceutical Sciences* **2024**, *203*, 106939. DOI: https://doi.org/10.1016/j.ejps.2024.106939.
(17) Messori, L.; Merlino, A. Cisplatin binding to proteins: A structural perspective. *Coordination Chemistry Reviews* **2016**, *315*, 67-89.
(18) Dos Santos, N. A. G.; Ferreira, R. S.; Dos Santos, A. C. Overview of cisplatin-induced neurotoxicity and ototoxicity, and the protective agents. *Food and chemical toxicology* **2020**, *136*, 111079.
(19) Miller, R. P.; Tadagavadi, R. K.; Ramesh, G.; Reeves, W. B. Mechanisms of Cisplatin nephrotoxicity. *Toxins (Basel)* **2010**, *2* (11), 2490-2518. DOI: 10.3390/toxins2112490 From NLM.
(20) Yu, M.; Lim, N. H.; Ellis, S.; Nagase, H.; Triccas, J. A.; Rutledge, P. J.; Todd, M. H. Incorporation of Bulky and Cationic Cyclam-Triazole Moieties into Marimastat Can Generate Potent MMP Inhibitory Activity without Inducing Cytotoxicity. *ChemistryOpen* **2013**, *2* (3), 99-105.
(21) Lau, Y. H.; Clegg, J. K.; Price, J. R.; Macquart, R. B.; Todd, M. H.; Rutledge, P. J. Molecular switches for any pH: a systematic study of the versatile coordination behaviour of cyclam scorpionands. *Chemistry–A European Journal* **2018**, *24* (7), 1573-1585.
(22) Héron, J.; Balcells, D. Concerted Cycloaddition Mechanism in the CuAAC Reaction Catalyzed by 1, 8-Naphthyridine Dicopper Complexes. *ACS Catalysis* **2022**, *12* (8), 4744-4753.
(23) Liang, L.; Astruc, D. The copper (I)-catalyzed alkyne-azide cycloaddition (CuAAC)"click" reaction and its applications. An overview. *Coordination Chemistry Reviews* **2011**, *255* (23-24), 2933-2945.
(24) Elattar, R. H.; El-Malla, S. F.; Kamal, A. H.; Mansour, F. R. Applications of metal complexes in analytical chemistry: A review article. *Coordination Chemistry Reviews* **2024**, *501*, 215568. DOI: https://doi.org/10.1016/j.ccr.2023.215568.
(25) Hulanicki, A.; Glab, S.; Ingman, F. Chemical sensors: definitions and classification. *Pure and applied chemistry* **1991**, *63* (9), 1247-1250.
(26) Petty, M. Applications of organised molecular films to electronic and opto-electronic devices. *Studies in Interface Science* **2002**, *16*, 317-367.
(27) Janata, J. *Principles of chemical sensors*; Springer Science & Business Media, 2010.
(28) Basabe-Desmonts, L.; Reinhoudt, D. N.; Crego-Calama, M. Design of fluorescent materials for chemical sensing. *Chemical Society Reviews* **2007**, *36* (6), 993-1017.
(29) Papadakis, R. Fluorescence Imaging: Recent Advances and Applications. **2023**.

(30) Pundi, A.; Chang, C.-J. Recent developments in the preparation, characterization, and applications of chemosensors for environmental pollutants detection. *Journal of Environmental Chemical Engineering* **2023**, 110346.
(31) Krämer, J.; Kang, R.; Grimm, L. M.; De Cola, L.; Picchetti, P.; Biedermann, F. Molecular probes, chemosensors, and nanosensors for optical detection of biorelevant molecules and ions in aqueous media and biofluids. *Chemical reviews* **2022**, *122* (3), 3459-3636.
(32) Snowden, T. S.; Anslyn, E. V. Anion recognition: synthetic receptors for anions and their application in sensors. *Current Opinion in Chemical Biology* **1999**, *3* (6), 740-746.
(33) Lewallen, D. M.; Hatch, D. M.; Iyer, S. S. Molecular Recognition Elements for Toxin and Pathogen Detection. *Chemosensors: Principles, Strategies, and Applications* **2011**, 455-474.
(34) Rosales-Vázquez, L. D.; Dorazco-González, A.; Sánchez-Mendieta, V. Efficient chemosensors for toxic pollutants based on photoluminescent Zn (II) and Cd (II) metal–organic networks. *Dalton Transactions* **2021**, *50* (13), 4470-4485.
(35) Aktar, M. W.; Sengupta, D.; Chowdhury, A. Impact of pesticides use in agriculture: their benefits and hazards. *Interdisciplinary toxicology* **2009**, *2* (1), 1.
(36) Graber, N.; Lüdi, H.; Widmer, H. The use of chemical sensors in industry. *Sensors and Actuators B: Chemical* **1990**, *1* (1-6), 239-243.
(37) Liang, X.; Sadler, P. J. Cyclam complexes and their applications in medicine. *Chemical Society Reviews* **2004**, *33* (4), 246-266.
(38) Hancock, R. D.; McDougall, G. J. The macrocyclic effect in tetraaza-macrocyclic ligands. *Advances in Molecular Relaxation and Interaction Processes* **1980**, *18* (2), 99-108.
(39) El Majzoub, A.; Cadiou, C.; Déchamps-Olivier, I.; Tinant, B.; Chuburu, F. Cyclam-methylbenzimidazole: a selective OFF-ON fluorescent sensor for zinc. *Inorganic chemistry* **2011**, *50* (9), 4029-4038.
(40) Demirbilek, M.; Pişkin, E. Effects of copper-cyclam and copper-cyclam/polymer complexes on HeLa cells. *Hacettepe Journal of Biology and Chemistry* **2008**, *36* (4), 263-271.
(41) Archana, B.; Sreedaran, S. New cyclam based Zn (II) complexes: effect of flexibility and para substitution on DNA binding, in vitro cytotoxic studies and antimicrobial activities. *Journal of Chemical Sciences* **2022**, *134* (4), 102.
(42) Voutsadaki, S.; Tsikalas, G. K.; Klontzas, E.; Froudakis, G. E.; Pergantis, S. A.; Demadis, K. D.; Katerinopoulos, H. E. A cyclam-type “turn on” fluorescent sensor selective for mercury ions in aqueous media. *RSC advances* **2012**, *2* (33), 12679-12682.
(43) Chen, J.; Li, Y.; Lv, K.; Zhong, W.; Wang, H.; Wu, Z.; Yi, P.; Jiang, J. Cyclam-functionalized carbon dots sensor for sensitive and selective detection of copper (II) ion and sulfide anion in aqueous media and its imaging in live cells. *Sensors and Actuators B: Chemical* **2016**, *224*, 298-306.
(44) Tamanini, E.; Katewa, A.; Sedger, L. M.; Todd, M. H.; Watkinson, M. A synthetically simple, click-generated cyclam-based zinc (II) sensor. *Inorganic Chemistry* **2009**, *48* (1), 319-324.

(45) Lau, Y. H.; Price, J. R.; Todd, M. H.; Rutledge, P. J. A Click Fluorophore Sensor that Can Distinguish CuII and HgII via Selective Anion-Induced Demetallation. *Chemistry–A European Journal* **2011**, *17* (10), 2850-2858.
(46) Ast, S.; Rutledge, P. J.; Todd, M. H. Reversing the Triazole Topology in a Cyclam-Triazole-Dye Ligand Gives a 10-Fold Brighter Signal Response to Zn2+ in Aqueous Solution. *European Journal of Inorganic Chemistry* **2012**, *2012* (34), 5611-5615.
(47) Ast, S.; Kuke, S.; Rutledge, P. J.; Todd, M. H. Using click chemistry to tune the properties and the fluorescence response mechanism of structurally similar probes for metal ions. *European Journal of Inorganic Chemistry* **2015**, *2015* (1), 58-66.
(48) Chivers, C. E.; Koner, A. L.; Lowe, E. D.; Howarth, M. How the biotin–streptavidin interaction was made even stronger: investigation via crystallography and a chimaeric tetramer. *Biochemical Journal* **2011**, *435* (1), 55-63.
(49) Yu, M.; Yu, Q.; Rutledge, P. J.; Todd, M. H. A fluorescent "allosteric scorpionand" complex visualizes a biological recognition event. *ChemBioChem* **2013**, *14* (2), 224-229.
(50) Gruber, H. J.; Marek, M.; Schindler, H.; Kaiser, K. Biotin− Fluorophore Conjugates with Poly (ethylene glycol) Spacers Retain Intense Fluorescence after Binding to Avidin and Streptavidin. *Bioconjugate chemistry* **1997**, *8* (4), 552-559.
(51) Wong, J. K. H.; Proschogo, N.; Todd, M. H.; Rutledge, P. J. Selective Displacement of a Scorpionand Triazole Ligand from Metallocyclam Complexes Visualised with NMR Spectroscopy. *European Journal of Inorganic Chemistry* **2017**, *2017* (7), 1075-1086.
(52) Olgun, A.; Oeztuerk, K.; Bayir, S.; Akman, S.; Erbil, M. K. Deuteronation and aging. *Annals of the New York Academy of Sciences* **2007**, *1100* (1), 400-403.
(53) Gerig, J. Fluorine NMR of proteins. *Progress in Nuclear Magnetic Resonance Spectroscopy* **1994**, *26*, 293-370.
(54) Worrell, B. T.; Hein, J. E.; Fokin, V. V. Halogen Exchange (Halex) Reaction of 5-Iodo-1, 2, 3-triazoles: Synthesis and Applications of 5-Fluorotriazoles. *Angewandte Chemie* **2012**, *124* (47), 11961-11964.
(55) Hein, J. E.; Tripp, J. C.; Krasnova, L. B.; Sharpless, K. B.; Fokin, V. V. Copper (I)-catalyzed cycloaddition of organic azides and 1-iodoalkynes. *Angewandte Chemie* **2009**, *121* (43), 8162-8165.
(56) Wang, D.; Sun, W.; Chu, T. Synthesis of 5-Fluorotriazoles by Silver-Mediated Fluorination of 5-Iodotriazoles. *European Journal of Organic Chemistry* **2015**, *2015* (19), 4114-4118.
(57) Arenas, J. L.; Retailleau, P.; Gillet, J.-M.; Ghermani, N.-E.; Ongeri, S.; Crousse, B. 5-Fluoro-1, 2, 3-triazole motif in peptides and its electronic properties. *Organic & Biomolecular Chemistry* **2022**, *20* (43), 8410-8414.
(58) Gan, H.; Oliver, A. G.; Smith, B. D. Fluorine NMR reporter for phosphate anions. *Chemical Communications* **2013**, *49* (44), 5070-5072.

(59) Xu, Z.; Zhao, Y. 19F-labeled molecular probes for NMR-based detection. *Journal of Fluorine Chemistry* **2023**, *266*, 110089.
(60) Kotková, Z.; Koucký, F.; Kotek, J.; Císařová, I.; Parker, D.; Hermann, P. Copper (ii) complexes of cyclams with N-(2, 2, 2-trifluoroethyl)-aminoalkyl pendant arms as potential probes for 19 F magnetic resonance imaging. *Dalton Transactions* **2023**, *52* (7), 1861-1875.
(61) Bech, A. G.; Health, A. I. o.; Welfare. *Breast Cancer in Australia: An Overview*; Australian Institute of Health and Welfare, 2012.
(62) Arnold, M.; Morgan, E.; Rumgay, H.; Mafra, A.; Singh, D.; Laversanne, M.; Vignat, J.; Gralow, J. R.; Cardoso, F.; Siesling, S.; Soerjomataram, I. Current and future burden of breast cancer: Global statistics for 2020 and 2040. *Breast* **2022**, *66*, 15-23. DOI: 10.1016/j.breast.2022.08.010 From NLM.
(63) O'Malley, B. W.; Khan, S. Elwood V. Jensen (1920-2012): father of the nuclear receptors. *Proc Natl Acad Sci U S A* **2013**, *110* (10), 3707-3708. DOI: 10.1073/pnas.1301566110 From NLM.
(64) Eyster, K. M. The Estrogen Receptors: An Overview from Different Perspectives. *Methods Mol Biol* **2016**, *1366*, 1-10. DOI: 10.1007/978-1-4939-3127-9_1 From NLM.
(65) Mahboobifard, F.; Pourgholami, M. H.; Jorjani, M.; Dargahi, L.; Amiri, M.; Sadeghi, S.; Tehrani, F. R. Estrogen as a key regulator of energy homeostasis and metabolic health. *Biomedicine & Pharmacotherapy* **2022**, *156*, 113808. DOI: https://doi.org/10.1016/j.biopha.2022.113808.
(66) Clusan, L.; Ferrière, F.; Flouriot, G.; Pakdel, F. A Basic Review on Estrogen Receptor Signaling Pathways in Breast Cancer. *Int J Mol Sci* **2023**, *24* (7). DOI: 10.3390/ijms24076834 From NLM.
(67) Tejería, M. E.; Pereira, M. P.; Gambini, J. P.; Duarte, P.; Giglio, J. G.; Rey, A. M. Synthesis of a [(18)F]F Estradiol Derivative via Click Chemistry Using an Automated Synthesis Module: In Vitro Evaluation as Potential Radiopharmaceutical for Breast Cancer Imaging. *Pharmaceuticals (Basel)* **2024**, *17* (3). DOI: 10.3390/ph17030388 From NLM.
(68) Miziak, P.; Baran, M.; Błaszczak, E.; Przybyszewska-Podstawka, A.; Kałafut, J.; Smok-Kalwat, J.; Dmoszyńska-Graniczka, M.; Kiełbus, M.; Stepulak, A. Estrogen Receptor Signaling in Breast Cancer. *Cancers (Basel)* **2023**, *15* (19). DOI: 10.3390/cancers15194689 From NLM.
(69) Hanstein, B.; Djahansouzi, S.; Dall, P.; Beckmann, M. W.; Bender, H. G. Insights into the molecular biology of the estrogen receptor define novel therapeutic targets for breast cancer. *European Journal of Endocrinology* **2004**, *150* (3), 243-255. DOI: 10.1530/eje.0.1500243 (acccessed 4/13/2025).
(70) Kiesewetter, D. O.; Kilbourn, M. R.; Landvatter, S. W.; Heiman, D. F.; Katzenellenbogen, J. A.; Welch, M. J. Preparation of four fluorine- 18-labeled estrogens and their selective uptakes in target tissues of immature rats. *J Nucl Med* **1984**, *25* (11), 1212-1221. From NLM.
(71) Lin, F. I.; Gonzalez, E. M.; Kummar, S.; Do, K.; Shih, J.; Adler, S.; Kurdziel, K. A.; Ton, A.; Turkbey, B.; Jacobs, P. M.; et al. Utility of (18)F-fluoroestradiol ((18)F-FES) PET/CT imaging as a pharmacodynamic marker in patients with refractory estrogen receptor-positive solid tumors receiving

Z-endoxifen therapy. *Eur J Nucl Med Mol Imaging* **2017**, *44* (3), 500-508. DOI: 10.1007/s00259-016-3561-8 From NLM.
(72) Pedersen, M. A.; Munk, O. L.; Dias, A. H.; Steffensen, J. H.; Møller, A. L.; Johnsson, A. L.; Hansen, K. V.; Bender, D.; Jakobsen, S.; Busk, M.; et al. Dynamic whole-body [(18)F]FES PET/CT increases lesion visibility in patients with metastatic breast cancer. *EJNMMI Res* **2024**, *14* (1), 24. DOI: 10.1186/s13550-024-01080-y From NLM.
(73) Alauddin, M. M. Positron emission tomography (PET) imaging with (18)F-based radiotracers. *Am J Nucl Med Mol Imaging* **2012**, *2* (1), 55-76. From NLM.
(74) Bourgoin-Voillard, S.; Fournier, F.; Afonso, C.; Zins, E.-L.; Jacquot, Y.; Pèpe, C.; Leclercq, G.; Tabet, J.-C. Electronic Effects of 11β Substituted 17β-Estradiol Derivatives and Instrumental Effects on the Relative Gas Phase Acidity. *Journal of the American Society for Mass Spectrometry* **2012**, *23* (12), 2167-2177. DOI: 10.1007/s13361-012-0486-8.
(75) Negi, A.; Kesari, K. K.; Voisin-Chiret, A. S. Estrogen Receptor-α Targeting: PROTACs, SNIPERs, Peptide-PROTACs, Antibody Conjugated PROTACs and SNIPERs. *Pharmaceutics* **2022**, *14* (11). DOI: 10.3390/pharmaceutics14112523 From NLM.
(76) Sedlák, D.; Eignerová, B.; Dračínský, M.; Janoušek, Z.; Bartůněk, P.; Kotora, M. Synthesis and evaluation of 17α-(carboranylalkyl)estradiols as ligands for estrogen receptors α and β. *Journal of Organometallic Chemistry* **2013**, *747*, 178-183. DOI: https://doi.org/10.1016/j.jorganchem.2013.06.013.
(77) Mansuri, S.; Ojha, S.; Kanvah, S. Targeted Imaging of Estrogen Receptor-Positive Cancer Cells Using Fluorescent Estradiol Probes. *Advanced Optical Materials* **2025**, *13* (8), 2402758. DOI: https://doi.org/10.1002/adom.202402758.
(78) Hanson, R. N.; Kirss, R.; McCaskill, E.; Hua, E.; Tongcharoensirikul, P.; Olmsted, S. L.; Labaree, D.; Hochberg, R. B. Targeting the estrogen receptor with metal-carbonyl derivatives of estradiol. *Bioorg Med Chem Lett* **2012**, *22* (4), 1670-1673. DOI: 10.1016/j.bmcl.2011.12.111 From NLM.
(79) Agami, C.; Couty, F. The reactivity of the N-Boc protecting group: an underrated feature. *Tetrahedron* **2002**, *58* (14), 2701-2724. DOI: https://doi.org/10.1016/S0040-4020(02)00131-X.
(80) Liu, J.-H.; Yang, C.-T.; Lu, X.-Y.; Zhang, Z.-Q.; Xu, L.; Cui, M.; Lu, X.; Xiao, B.; Fu, Y.; Liu, L. Copper-Catalyzed Reductive Cross-Coupling of Nonactivated Alkyl Tosylates and Mesylates with Alkyl and Aryl Bromides. *Chemistry – A European Journal* **2014**, *20* (47), 15334-15338. DOI: https://doi.org/10.1002/chem.201405223.
(81) Bosnich, B.; Poon, C. K.; Tobe, M. L. Complexes of Cobalt(III) with a Cyclic Tetradentate Secondary Amine. *Inorganic Chemistry* **1965**, *4* (8), 1102-1108. DOI: 10.1021/ic50030a003.
(82) Maimon, E.; Zilbermann, I.; Cohen, H.; Kost, D.; van Eldik, R.; Meyerstein, D. Mechanism of Isomerization of Ni(cyclam) in Aqueous Solutions. *European Journal of Inorganic Chemistry* **2005**, *2005* (24), 4997-5004. DOI: https://doi.org/10.1002/ejic.200500523.

(83) Liang, X.; Weishäupl, M.; Parkinson, J. A.; Parsons, S.; McGregor, P. A.; Sadler, P. J. Selective Recognition of Configurational Substates of Zinc Cyclam by Carboxylates: Implications for the Design and Mechanism of Action of Anti-HIV Agents. *Chemistry – A European Journal* **2003**, *9* (19), 4709-4717. DOI: https://doi.org/10.1002/chem.200304808.
(84) Lelong, E.; Suh, J.-M.; Kim, G.; Esteban-Gómez, D.; Cordier, M.; Lim, M. H.; Delgado, R.; Royal, G.; Platas-Iglesias, C.; Bernard, H.; Tripier, R. Complexation of C-Functionalized Cyclams with Copper(II) and Zinc(II): Similarities and Changes When Compared to Parent Cyclam Analogues. *Inorganic Chemistry* **2021**, *60* (15), 10857-10872. DOI: 10.1021/acs.inorgchem.1c01572.
(85) Laszlo, P. Chapter 6 Solvent effects and nuclear magnetic resonance. *Progress in Nuclear Magnetic Resonance Spectroscopy* **1967**, *3*, 231-402. DOI: https://doi.org/10.1016/0079-6565(67)80016-5.
(86) Alfonso, I.; Astorga, C.; Rebolledo, F.; Gotor, V.; García-Granda, S.; Tesouro, A. Structural studies of two protonated forms of a C2 symmetrical optically active cyclam derivative. *Journal of the Chemical Society, Perkin Transactions 2* **2000**, (4), 899-904, 10.1039/A904998C. DOI: 10.1039/A904998C.
(87) Lindon, J. C. NUCLEAR MAGNETIC RESONANCE SPECTROSCOPY-APPLICABLE ELEMENTS | Fluorine-19. In *Encyclopedia of Analytical Science (Second Edition)*, Worsfold, P., Townshend, A., Poole, C. Eds.; Elsevier, 2005; pp 263-272.
(88) Hore, P. Nuclear Magnetic Resonance. *(No Title)* **2015**, 34.
(89) Rosenau, C. P.; Jelier, B. J.; Gossert, A. D.; Togni, A. Exposing the Origins of Irreproducibility in Fluorine NMR Spectroscopy. *Angewandte Chemie International Edition* **2018**, *57* (30), 9528-9533. DOI: https://doi.org/10.1002/anie.201802620.
(90) Jaouen, K.; Szpak, P.; Richards, M. P. Zinc Isotope Ratios as Indicators of Diet and Trophic Level in Arctic Marine Mammals. (1932-6203 (Electronic)). From 2016.
(91) Meyerson, S. Natural Abundance of Chlorine Isotopes. *Analytical Chemistry* **1961**, *33* (7), 964-964. DOI: 10.1021/ac60175a046.
(92) Tajima, S.; Ueki, M.; Tajima, S.; Sekiguchi, O.; Shigihara, A. Unimolecular HF Loss from the Molecular Ions of Fluorophenols and Fluoroanilines. A 'Ring-walk' Mechanism of a Fluorine Atom. *Rapid Communications in Mass Spectrometry* **1996**, *10* (9), 1076-1078. DOI: https://doi.org/10.1002/(SICI)1097-0231(19960715)10:9<1076::AID-RCM621>3.0.CO;2-5.
(93) Giorgi, G.; Palumbo Piccionello, A.; Pace, A.; Buscemi, S. Effect of Protonation and Deprotonation on the Gas-Phase Reactivity of Fluorinated 1,2,4-Triazines. *Journal of the American Society for Mass Spectrometry* **2008**, *19* (5), 686-694. DOI: https://doi.org/10.1016/j.jasms.2008.01.014.
(94) Liu, X.-C.; Lin, L. Controlling the Self-Assembly of Metal-Cages organic and transdermal drug delivery. *Inorganic Chemistry Communications* **2021**, *129*, 108660. DOI: https://doi.org/10.1016/j.inoche.2021.108660.

(95) Chernobryva, M.; Motevalli, M.; Hawes, C. S.; Watkinson, M. An investigation into the coordination chemistry of tripodal "click" triazole ligands with Mn, Ni, Co and Zn ions. *Journal of Molecular Structure* **2022**, *1259*, 132736. DOI: https://doi.org/10.1016/j.molstruc.2022.132736.
(96) Keypour, H.; Shayesteh, M.; Salehzadeh, S.; Dhers, S.; Maleki, F.; Ünver, H.; Dilek, N. Probing the effect of arm length and inter- and intramolecular interactions in the formation of Cu(ii) complexes of Schiff base ligands derived from some unsymmetrical tripodal amines. *New Journal of Chemistry* **2015**, *39* (9), 7429-7441, 10.1039/C5NJ01318F. DOI: 10.1039/C5NJ01318F.
(97) Tabbì, G.; Giuffrida, A.; Bonomo, R. P. Determination of formal redox potentials in aqueous solution of copper(II) complexes with ligands having nitrogen and oxygen donor atoms and comparison with their EPR and UV–Vis spectral features. *Journal of Inorganic Biochemistry* **2013**, *128*, 137-145. DOI: https://doi.org/10.1016/j.jinorgbio.2013.07.035.
(98) Brown, C. J. M. Target-Activated Metal Complexes for Imaging the Estrogen Receptor. University of Sydney 2016.
(99) Zhu, Z.; Chen, H.; Li, S.; Yang, X.; Bittner, E.; Cai, C. Tripodal amine ligands for accelerating Cu-catalyzed azide–alkyne cycloaddition: efficiency and stability against oxidation and dissociation. *Catalysis Science & Technology* **2017**, *7* (12), 2474-2485, 10.1039/C7CY00587C. DOI: 10.1039/C7CY00587C.
(100) Díez-González, S.; Correa, A.; Cavallo, L.; Nolan, S. P. (NHC)Copper(I)-Catalyzed [3+2] Cycloaddition of Azides and Mono- or Disubstituted Alkynes. *Chemistry – A European Journal* **2006**, *12* (29), 7558-7564. DOI: https://doi.org/10.1002/chem.200600961.
(101) Fabbrizzi, L.; Foti, F.; Licchelli, M.; Maccarini, P. M.; Sacchi, D.; Zema, M. Light-Emitting Molecular Machines: pH-Induced Intramolecular Motions in a Fluorescent Nickel(II) Scorpionate Complex. *Chemistry – A European Journal* **2002**, *8* (21), 4965-4972. DOI: https://doi.org/10.1002/1521-3765(20021104)8:21<4965::AID-CHEM4965>3.0.CO;2-X.
(102) Demko, Z. P.; Sharpless, K. B. An Intramolecular [2 + 3] Cycloaddition Route to Fused 5-Heterosubstituted Tetrazoles. *Organic Letters* **2001**, *3* (25), 4091-4094. DOI: 10.1021/ol010220x.
(103) Hein, J. E.; Tripp, J. C.; Krasnova, L. B.; Sharpless, K. B.; Fokin, V. V. Copper(I)-Catalyzed Cycloaddition of Organic Azides and 1-Iodoalkynes. *Angewandte Chemie International Edition* **2009**, *48* (43), 8018-8021. DOI: https://doi.org/10.1002/anie.200903558.
(104) Takahashi, A. Role of zinc and copper in erythropoiesis in patients on hemodialysis. *Journal of Renal Nutrition* **2022**, *32* (6), 650-657.
(105) Montierth, J. M.; DeMario, D. R.; Kurth, M. J.; Schore, N. E. The polymer-supported Cadiot-Chodkiewicz coupling of acetylenes to produce unsymmetrical diynes. *Tetrahedron* **1998**, *54* (39), 11741-11748. DOI: https://doi.org/10.1016/S0040-4020(98)83035-4.